CHALMERS
UNIVERSITY OF TECHNOLOGY

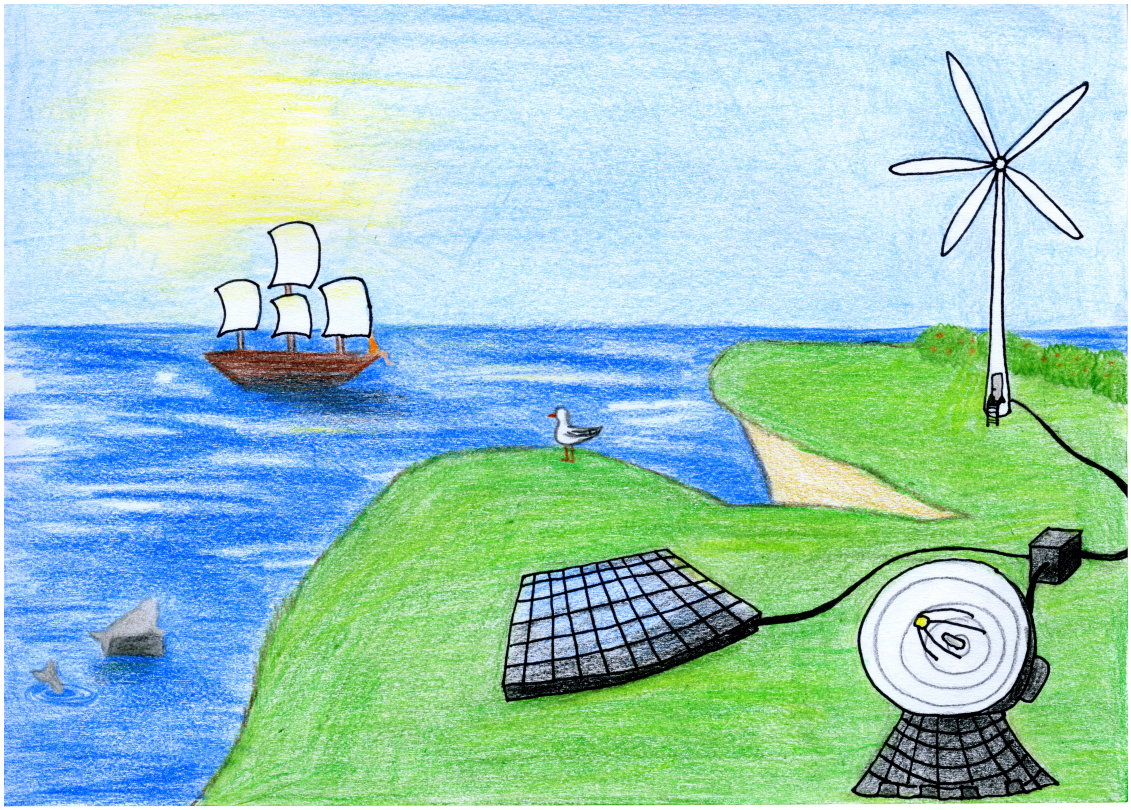

An Off-grid Energy Harvesting System for Radar Equipment

Master's thesis in Electrical Power Engineering

NIKLAS BLOMKVIST
VICTOR LOFTMAN

Department of Energy and Environment
CHALMERS UNIVERSITY OF TECHNOLOGY
Gothenburg, Sweden 2019

Master's thesis 2019

An Off-grid Energy Harvesting System for Radar Equipment

NIKLAS BLOMKVIST AND VICTOR LOFTMAN

CHALMERS
UNIVERSITY OF TECHNOLOGY

Department of Energy and Environment
Division of Electrical Power Engineering
Chalmers University of Technology
Gothenburg, Sweden 2019

An Off-grid Energy Harvesting System for Radar Equipment
NIKLAS BLOMKVIST AND VICTOR LOFTMAN

Supervisor: Niklas Janehag, SAAB AB and Valter Nilsson, SAAB AB
Examiner: Torbjörn Thiringer, Department of Energy and Environment

Master's Thesis 2019
Department of Energy and Environment
Division of Electrical Power Engineering
Chalmers University of Technology
SE-412 96 Gothenburg
Telephone +46 31 772 1000

Cover: An energy harvesting system by the coast.
By: Agnes Juhlin, Hjärnarp, Sweden, 2019.

Typeset in LaTeX
Gothenburg, Sweden 2019

An Off-grid Energy Harvesting System for Sensor Equipment
NIKLAS BLOMKVIST AND VICTOR LOFTMAN
Department of Energy and Environment
Chalmers University of Technology

Abstract

This thesis investigates the possibility of using an off-grid energy harvesting system to supply a radar with a power output of $260W$. The system is designed after three different locations: Gothenburg/Sweden, Sde Boker/Israel and Thule/Greenland. The most suitable energy sources were photovoltaic cells and wind turbines, and additionally an energy storage system of lithium iron phosphate batteries was used. Models based upon theses technologies are made to be able to investigate different systems and locations.

Three converters were designed to maintain the required voltage levels and to suppress the voltage and the current ripple. All converters were designed in `LTSpice`. The designed converters are: a buck converter at the solar cells, a boost converter at the wind turbine and a bidirectional converter at the battery. Finally, snubber circuits were added to the semiconductors to reduce the electrical stresses and potentially reduce the losses. The efficiency of each converter were used in the complete system simulation.

By modeling the system in `Simulink` with historical weather data, from the selected locations, the system were sized properly and optimized for each location. In Gothenburg, the optimal system included a combination of solar power and wind turbines to achieve a denser power production. In the desert area, Sde Boker, the solar power was dominant and the system could be scaled down in comparison to Gothenburg but wind turbine could contribute to reduce the system cost. For Thule, the climate were a problem and a wind turbine system is to be preferred. The final results are based upon a trade-off between the size and the cost of the system.

Keywords: Energy Harvesting System, Off-grid , Wind Power, Solar Power, Radar, Power Converter, Snubbers, Renewable Energy

Acknowledgements

Words are not enough to express the gratitude we have toward out supervisors. Niklas Janehag and Valter Nilsson at SAAB have provided us with many interesting discussions which have helped form the project. Through their guidance we were able to easily overcome many complicated issues.

We would also like to thank Martin Sydstrand at SAAB for all his help in the start of the project. With Martin's help, all software and license related issues were able to be solved in a simple and fast way. The start of a project is usually the most important part and thanks to Martin's help, we were able to start the project in a smooth way.

We further wish to extend our gratitude to Anthony Norman at the division of language and communication at Chalmers for providing guidance regarding the structure of the report and grammatical formulations. His help improved the report and opened new doors for us of how to express ourself.

Lastly, we wish to extend our warmest thanks to SAAB's department of digital and power electronics for the wonderful time we have spent with them. The affinity and welcome you have given us during our time at the company have exceeded all our expectations. The time spent at the company and outside of the company have included many fun moments and memories. We are also grateful to the group for all the advice and suggestions you have provided to help us improve our project.

Victor Loftman and Niklas Blomkvist, Gothenburg, June 2019

Contents

1
Introduction

In this chapter, an introduction to why off-grid energy harvesting systems are of interest is presented. An aim and a scope are also presented to pinpoint what is included and what is not included in the report. Finally, the methodology of how the work was conducted is described.

1.1 Background

In a world where electrification and access to electric power is necessary in most applications, possible power generating solutions are essential. In urban areas, accessibility of electricity is usually high, but in areas located far from cities or locations which are connected to the power grid, access can be problematic. Transferring electricity to remote areas that are without direct access can be problematic and costly, due to the need for grid extensions and infrastructure planning [1], [2]. The initial cost of extending a grid to rural areas is higher than installing an energy harvesting system [1]. Electrification of areas which have poor to no connection to the existing power grid is the primary reason why development of off-grid systems has increased [3], [4]. A large percentage of citizens in developing countries do not have access to the power grid and here off-grid technologies are a suitable choice [3], [5]. A benefit of utilizing an energy harvesting system is the environmental aspect. As only renewable energy sources are used, no fossil fuels are consumed, which limits the environmental footprint of the system.

Another reason why off-grid energy harvesting systems for radars are of interest is dut to the need for independent operation. Accessibility to the system may be limited by environmental factors such as poor connections or lack of available personnel at the location. For the system to be self-sustainable and independent, renewable energy sources are mainly used as no fuel is needed and require low maintenance [6], [7]. There are several studies that have analyzed off-grid systems which use renewable energy sources [8]–[11] and not any conventional fossil power generation. An off-grid harvesting system can use one or multiple source(s) of power and possible sources are wind-, wave- and solar power [1], [8]. Depending on the location and the environmental situation, different alternatives can be more relevant compared to others. Therefore, an optimized system may not only include one generating source of power.

An application area which is possible due to the increased interest and development,

is the use of radars located in rural locations. Positions like coastal areas or mountains can be of interest for data gathering, for the sake of safety and surveillance. An advantage can be to limit the interference from the environment on the radar beam so the collected data is of higher quality [12]. With continued advancement in semi-conducting technologies, radar systems can operate without moving parts and have reduced losses [13], [14]. Small scale radar systems which usually require small amount of energy can therefore be feasible for these applications. This may also increase the feasibility of portable radar systems. Finally, as radar systems may require continuous operation, an energy storage system (ESS) is connected to the system to ensure that the system have the required power.

Implementation of energy harvesting systems connected to homes have seen an increase in interest as the availability and affordability of solar solar cells are better. A household in Agnesberg, Gothenburg have built a system which is self sustainable and include solar cells, a large battery and hydrogen tanks. By storing hydrogen, the system is able to aid with power and heating demand during the winter[1].

1.2 Aim

The aim of this report is to design an energy harvesting systems for a radar, with a maximum power of $260W$. The system should be able to supply the required power depending on the chosen operation mode of the radar. Three different environments and two radar operation modes are divided in cases where a solution for each needs to be found. Finally, the report aims to provide system recommendations for one of the investigated locations.

The energy production comes from one or multiple renewable energy source(s), which are decided based upon the location. Due to renewable energy production varying characteristics, an ESS is also investigated to minimize the impact of the variations in power generation. Thereafter, power electronics converters are to be designed to link the production with the ESS and the radar.

1.3 Scope

The report include the design of energy harvesting systems for three different environments. Additionally, two different modes of operation for the radar are evaluated for each location. The system is simulated over several years with historical weather data and the results trustworthiness is dependent on the validity of the weather data.

Power production technologies and an ESS are selected and designed based upon their potential at the location, sustainable aspects, occupied area and cost. The

[1] https://www.nyteknik.se/nyheter/fri-fran-elnatet-med-egen-vatgas-6344197 D.O.A: 2019:05:21

design of the radar is not included in the report. From the product sheet, the voltage and power input requirements are given. No power generating products will be designed and existing products will be used and models are designed to mimic existing products.

A circuit design of the converters in the system are presented in the report with its related snubber design. The components used in the circuit simulation software are assumed to be representing reality and parasitic elements are estimated.

The control of the system is not included in the report. For the simulations, the control of converters are assumed to be working perfectly. Additionally, the maximum power point tracker and the yaw controller for the solar power and the wind turbines are presumed. Finally, a battery management system is also assumed to handle temperature and charge level.

1.4 Problem definition

The report aims to analyze and evaluate energy harvesting systems which are able to provide enough power to meet the demand of a radar in a self-sustainable way. To accomplish this, renewable energy sources were selected and evaluated based upon the environments of interest. For the evaluation to be trustworthy, weather measurements were used for the models. The sustainable energy sources are dependent on the available weather data, and therefore gather data of high quality was of importance.

For the project, two different modes were investigated. One mode is a continuous mode of operation while the other is an interval mode. To ensure that there is always enough power to operate the radar, an ESS was investigated. For the selection of ESS, an evaluation will be carried out to select the most adequate system. Criterias, which are of interest, are: required energy- and power density, robustness, temperature stability, cost and life length.

When connecting different subsystems to generate a full model, power electronics are needed. The power electronic converters need to be designed to meet the requirements and be able to keep the load at its rated voltage level. The electrical stress and losses of these converter needs to be investigated and snubbers are designed for them to finalize the full model.

1.4.1 Environments and Locations Under Investigation

For the project, three different environment are investigated and plausible systems will be estimated from the simulations. The first environment selected is the west coast of Sweden, Gothenburg. This is the location where the project was carried out and is the city of where Chalmers University of Technology is located. Secondly, the southern desert area of Israel, Sde Boker, was selected because this place is located at latitudes close to the equator and hence have high solar radiation over

the entire year. Thirdly, the small town of Thule, which is located in the northwest of Greenland, was selected. The interesting part with Thule is the fact that during the summer the sun never sets and during the winter it disappears for a few month, which brings extreme cold temperatures. All locations can be seen in the map in figure 1.1.

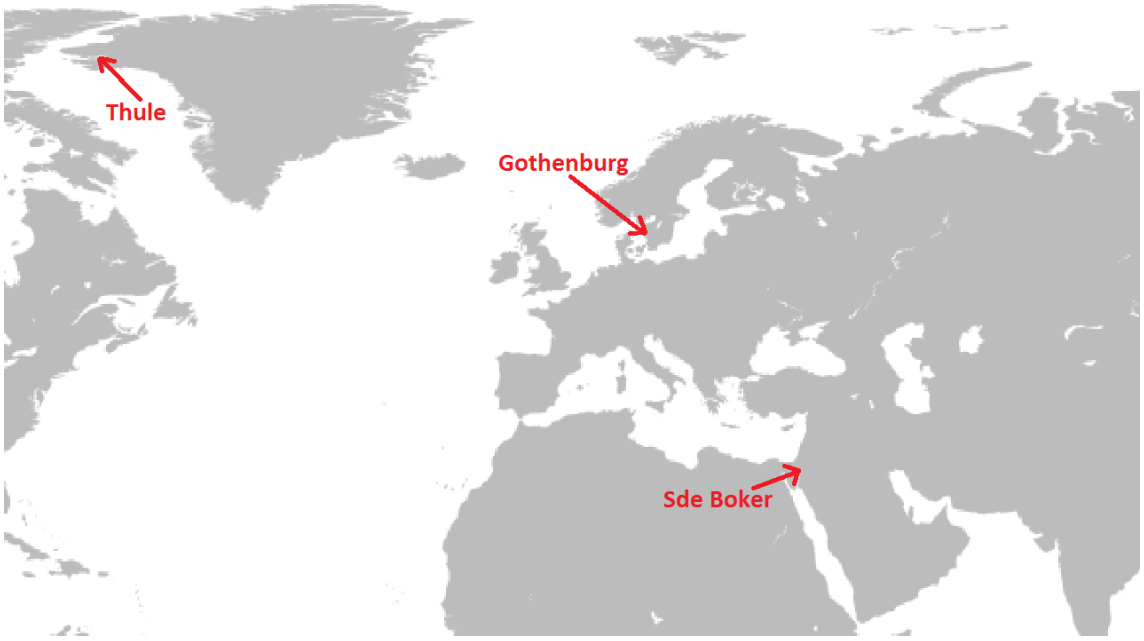

Figure 1.1: Map of the locations selected.

1.5 Methodology

This project was conducted by doing a background theory research of previous similar projects to gain a deeper knowledge within some key areas that the project includes. With this information, how the rest of the work should be conducted, was planned. Investigations were needed for evaluating which technologies that are the most appropriate choice(s) for different environmental scenarios. The evaluation took available energy sources, ESS and power electronics into consideration so they meet the requirements for each scenario. Finally, a sustainable aspect which involved a social, a economical and a environmental perspective was included to make system design choices.

The next step was calculations and simulations of the system. First, design of each individual component was carried out and a larger system was constructed in a later stage, by adding the essential components together. For the simulation of the power electronics, `LTSpice` was primary used. The time frame which power electronics are simulated are usually shorter than a few seconds, and therefore it was not suitable to simulate the entire system in `LTSpice` as it may use a time frame of entire months. Using longer periods of time, how the system handle transient changes can be analyzed. For these simulations, `MATLAB`© and `Simulink` were used.

1.5.1 Code of Ethics

The project have taken ethic aspects into consideration and the work process have followed the guidelines given from IEEE. From these principles, some are presented in this section to understand the implication of ethics for this project.

The first ethic guideline is, to be honest and realistic in stating claims or estimates based on available data. As the project uses renewable energy sources, available data and the quality of the data is essential. Hence, the need to be critical and consider the trustworthiness of the data is of importance for the result to be unbiased. The project is conducted at SAAB AB©, who expect an in-depth analysis of the problem for future interest and thus, there should be no concern regarding the trustworthiness of the result which is presented.

Working towards a company as SAAB AB©, that is influenced by income, could lead to that one overestimates quality of the design and do not make honest and realistic claims of certain specifics regarding the project. The project is desired to be a realistic model and thus, unrealistic claims are not accepted, as it may cause decreased reliability and quality for the final product.

One guideline in the IEEE code of ethics is to not discriminate any persons based of religion, gender, disability, age, national origin, sexual orientation, gender identity, or gender expression. As the report aimed to be objective, and coworkers treated with respect, this was not a problem.

Another ethic guideline is, to seek, accept, and offer honest criticism of technical work, to acknowledge and correct errors, and to properly credit the contributions of other. To be able to finish the project and form such a complete understanding as possible, outside information and input was required. By right, the original author or person who have helped, have receive acknowledgment for the contribution. Additionally, criticism which is directed towards the project has been warmly welcome as it helped to improve the quality of the the project. Finally, the criticism offered from the group had a good motivation so the receiver could understand the reason behind the claim.

2
Theory

In this chapter, relevant technologies which are used in energy harvesting systems are presented. How the different technologies can be modeled are included to be able to investigate their feasibility to be used in the off-grid.

2.1 Energy Harvesting System

In electric grids, there are many types of energy production. For small-scale off-grid systems, wind and solar power are commonly combined for a more continuous production [15]. Renewable energy sources require better day-ahead scheduling management due to weather variations [16]. This leads to a need to oversize the system to guarantee that there is enough energy in the system or to use an ESS.

2.2 Solar Power Generation

There are two primary methods for harvesting solar energy: concentrated solar power (CSP) systems and photovoltaic (PV) cell systems. The methods are based on different principles, which will be discussed in the following section. Ancillary components will be included to provide additional background for each method.

2.2.1 Concentrated Solar Power

A common CSP technology is parabolic through collector (PTC) systems. This technology have been in development for a long time and can be considered mature. Figure 2.1 displays how a PTC collector can look. The power generating principle of a PTC system is that sunlight shines on a half circle and is reflected to a receiver in the centre [17]. The receiver contains a fluid which gets vaporized and transferred to a generator. This system therefore requires a large amount of liquid and occupies large areas.

Solar power towers (SPT) utilize flat mirrors, heliostats, to reflect sunlight toward a tower. The tower act as the receiver and absorb the reflected sunlight. The conversion process is the same as in PTC. An SPT has a high efficiency compared to PTC but is more expensive [18]. Additionally, a linear Fresnel reflector (LFR) is based on the same topology as PTC but uses an independent receiver which collects the reflected sunlight. For LFR, the mirrors are flat and compared to curved mirrors, flat surfaces are cheaper to produce. Because of the mirrors, LFR systems are less

expensive than PTC systems of the same size. An LFR has common points with both the PTC and the SPT system, and the design is similar to a combination of the two systems [19].

Lastly, parabolic dish collector (PDC) systems use pin-point reflection, so the heat can reach high levels at a single point. It is a newer technology which has high requirements on reflectors, tracking systems and heat conduction [19]. PDC is therefore an expensive technology, due to the expensive ancillary components.

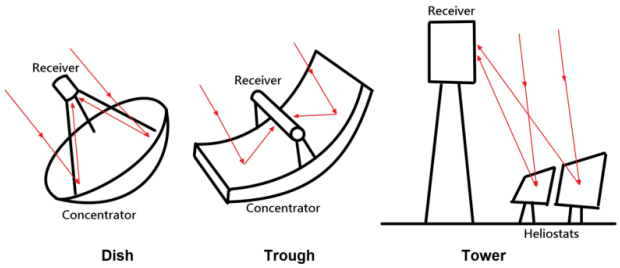

Figure 2.1: How the different CSP technologies compare to each other and the structural disparities [20]. CC-BY-NC-SA

2.2.2 Silicon Photovoltaic (PV) Cells

Silicon PV cells can be divided depending on the atomic structure of the cell. Mono crystalline cells have a close to flawless atomic structure and poly crystalline have more defects in its atomic structure. Amorphous PV cells are shapeless and it can be complicated to find a structure in the atomic alignment. As the atomic structure is less flawed, the efficiency and cost increases; therefore, mono crystalline cells are the most expensive and have the highest efficiency. Table 2.1 displays how different silicon PV cells are compared to each other.

Table 2.1: How different Silicon PV cells compare to each other [21], [22].

Silicon structure	Mono	Poly	Amorphous
Atomic structure	≈Perfect	Exist impurities	Shapeless
Efficiency	20-25%	14-19%	5-7%
Cost	High	Moderate	Low

PV cells convert solar energy to electricity directly, and uses the excitation of electrons as the working principle [23]. The solar energy excites electrons in the PV material, which start to drift. The current which is generated from the PV cells are directly related to the electron drift.

2.2.2.1 PV Power Generation

A PV cell can be modeled as a current source as it generates a drift current. Additionally, a shunt (R_{sh})- and a series (R_s) resistance are needed to include the leakage

current and material resistances in the cell respectively [24]. A PV cell consists of p-n junctions, and as a diodes' basic principle builds upon p-n junctions, a diode is included to simulate this effect. The proposed circuit design can be seen in figure 2.2 and the described parts are present and can be pinpointed.

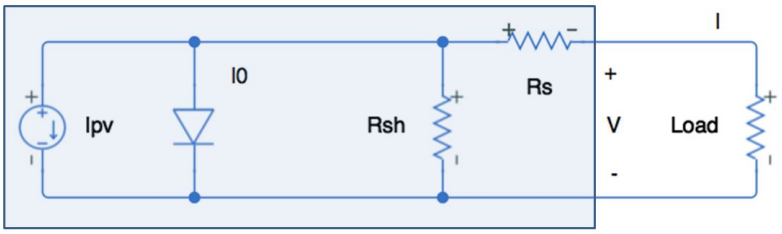

Figure 2.2: Displays the equivalent circuit for a PV cell and what components that are included. The marked area pinpoint what is related to the PV circuit.

From figure 2.2, an expression for the output current can be found. This expression can be written as

$$I = I_{pv} - I_0 \left(e^{\frac{V+IR_s}{nV_T}} - 1 \right) - \frac{V + IR_s}{R_{sh}} \tag{2.1}$$

In (2.1), I represent the output current, I_{pv} is the current which the cell is generating, I_0 is the reverse diode saturation current, V is the output voltage, n represent the diode ideality factor and V_T is a temperature dependent factor. By plotting the expression with respect to the output voltage, the maximum output power which the solar cell can generate, can be found. Figure 2.3 displays that the maximum power point can be found in the right corner of the plot. The marked area is the maximum generated power which is important to find. Therefore, a maximum power point tracker (MPPT) is usually implemented to assist with this task. An MPPT also help to handle variations in irradiation. For each PV cell, there exist a temperature dependence which describe how the power output change at cell temperatures over the normal operating cell temperature (NOCT)[2], and the power output decrease with increase temperature.

Essentially, the output current from a solar cell is proportional to the sun irradiation at each instant. Due to resistances in the circuit, this relationship is not applicable to the entire range and can primary be used at I_{sc}. The short circuit current can be expressed as

$$I_{sc} = I_{scNOCT} \frac{G}{G_{NOCT}}, \tag{2.2}$$

where I_{scNOCT} is the output current at NOCT conditions, I_{sc} is the new short circuit current due to change in irradiation, G represent the irradiation at the given moment and finally, G_{NOCT} is the irradiation at NOCT conditions. As for the voltage, it can be noted from (2.1) that the open circuit voltage, V_{oc}, can expressed with a logarithmic relationship. A realization off V_{oc} can be expressed in the following way,

[2]Normal Operating Cell Temperature conditions: G = $800W/m^2$, T = 20°C, wind velocity = 1m/s. Represent a more realistic test for the PV cells.

$$V_{oc} = V_{ocNOCT} + nV_T \cdot ln\left(\frac{G}{G_{NOCT}}\right), \tag{2.3}$$

and from (2.3), V_{oc} is the cell's open circuit voltage and V_{ocNOCT} represent the open circuit voltage at NOCT conditions.

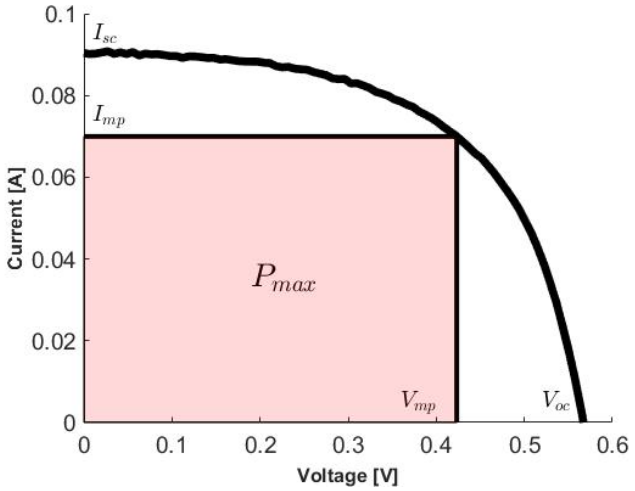

Figure 2.3: Display the implicit equation for the output current with respect to the output voltage. Presented is the IV curve for a mono crystalline silicon PV cell. The marked area is the maximum power which can be generated from the cell.

To find the MPPT point in figure 2.3, a MPPT is used. One of the main methods which can be used is the perturb and observe ($P\&O$) method. $P\&O$'s principle is to analyze the voltage and the current at a point in time and compare it with the prior point. When increasing the voltage, if the product of the new point is higher than the previous point, the voltage should be increased further. In the opposite case, the voltage should decrease instead [25]. The flowchart of the method is displayed in figure 2.4 and it can be seen that it is needed to compare different points before it is possible to find the optimal point [25].

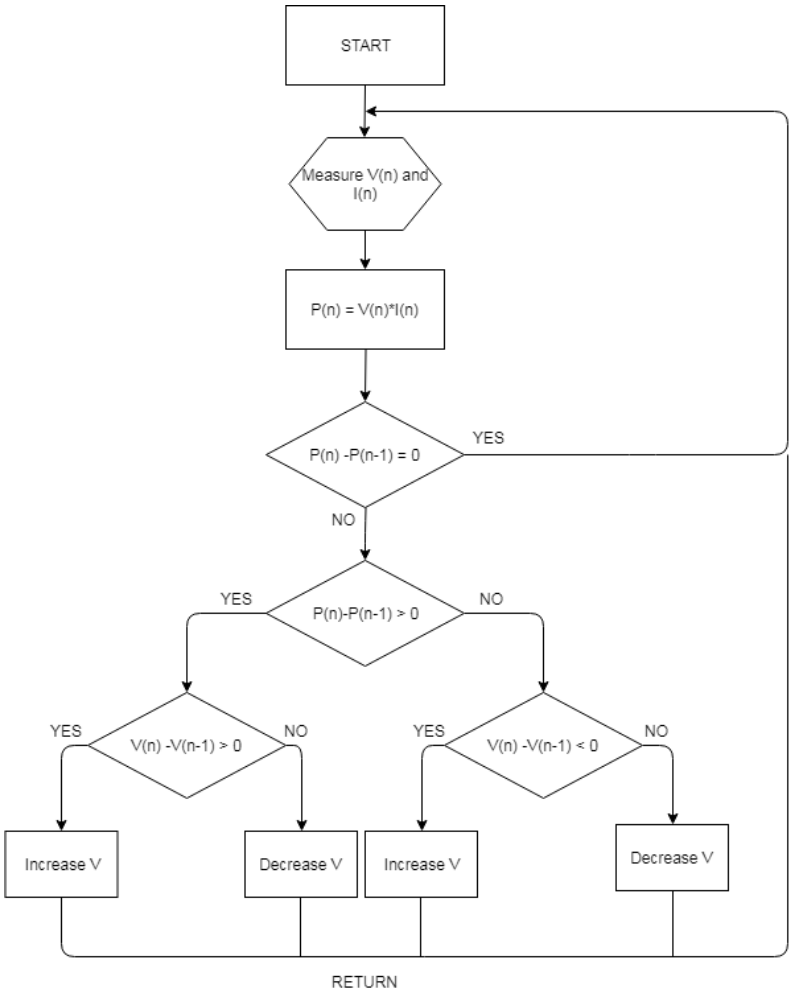

Figure 2.4: Flowchart of the *P&O* method.

2.3 Wind Power

Wind turbines are divided into two sub-categories: horizontal-axis wind turbines (HAWT) and vertical-axis wind turbines (VAWT). For large scale wind farms, the most commonly used design is the HAWT three blade design but for smaller scale systems, VAWTs becomes a viable option [26]. In figure 2.5a a three blade HAWT can be seen and it can be of large size. A VAWT, which can be seen in figure 2.5b, can be installed in residential areas and do not occupy large amount of area. The presented VAWT design is one of many possible designs, but the general principle will remain the same throughout for all VAWTs.

(a) How a $1.6MW$ HAWT may look like [27] CC-BY-SA.

(b) A $6kW$ VAWT in a residential area [28] CC-BY-SA.

Figure 2.5: General design of a HAWT and a VAWT.

The efficiency of a HAWT compared to a VAWT is generally higher and is thus the more commonly used design. Additionally, a HAWT is easier to scale up and is therefore more affordable if large amount of energy need to produced [26], [29], [30]. However, VAWTs are independent of the wind direction and have an lower cut-in wind speed, which result in a higher power density due to turbulance can be utilized [26]. The placement of HAWTs are of higher importance because of this. In table 2.2, a comparison between vertical- and horizontal axis turbines is presented. The comparison is generalized, especially the cost since the VAWTs can use more types of winds and the rated operation point is different for various turbines.

Table 2.2: Comparison between vertical- and horizontal axis turbine.

	VAWTs	HAWTs
Efficiency	Poor	Good
Wind direction	Independent	Dependent
Cost/Rated power	High	Low

In cold climates, wind turbines are troubled by ice which form on the blades and the rest of the turbine (icing). Icing exposes the wind turbine to excessive stress and decrease the performance, or even halts it. If the temperature at a location fulfills the nine-day critera; nine consecutive days with at least one hour of temperatures below

-20°C, an ice preventing system need to be used. The system can be implemented into the blades, so the blades are heated up and melting the ice [31]. Unfortunately, an ice preventing system will require additional power from the system.

2.3.1 Wind Power Generation

A general equation used to estimate the power output of a wind turbine is the wind power equation

$$P = \frac{1}{2} C_p \rho A_{swept} v^3, \tag{2.4}$$

where C_p is the maximum power coefficient, ρ is the air density, A_{swept} is the swept area and v is the wind speed. C_p is not a constant but varies with different wind speeds [32]. At low and high wind speeds, wind turbines can not operate efficient. Until the wind speed reaches the cut-in speed or drops below its cut-out speed, no power is produced. Figure 2.6 displays the power output from wind turbines with different blade radius, r, according to (2.4). The power is limited at high wind speed due to the risk of turbine damages. Since $A_{swept} \propto r^2$ for HAWTs, the power increases with size.

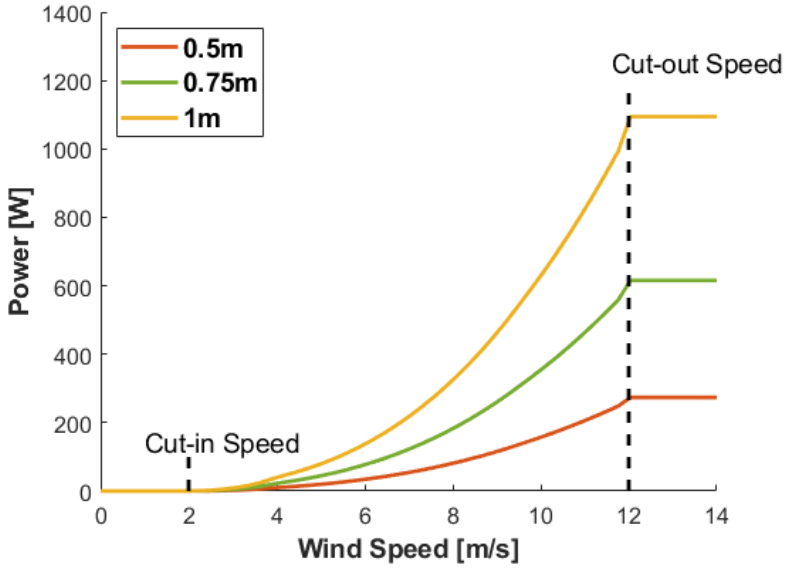

Figure 2.6: The wind power equation at three different blade radius and a limited power output at high wind speeds.

2.3.2 Yaw Control

When comparing the rated power of a HAWT with a VAWT, a fair result is not obtained. HAWTs assumes that the wind enters the swept area perpendicular. Since the VAWTs are independent from the wind speed's direction it can generate power from turbulence close to the ground. As a HAWT produce the most power when the wind direction is perpendicular to the blades, it is necessary to alter the blades

direction to match the wind direction. This can be done with a mechanical gear that control the direction the wind turbine face. The control is called yaw control.

Yaw control can be done in an active- or a passive way. Using a control schematic and sense the wind direction and thereafter change how the turbines should be altered is an active way of yaw control. Passive yaw control can be a tail connected to the turbine. The wind will push the turbine, the tail in particular, until it is perpendicular to the wind direction [33], [34]. An error is associated with both the mentioned control schematics and the error relate how precise the wind turbine can follow the wind direction. The error is usually represented with a factor, $cos(\theta)$, where θ is the angle between the wind turbine and wind direction. The lower allowed angle tolerance, the more precise can the wind tracking be done and more power can be generated [35]. The error factor is then multiplied to the wind power equation, (2.4), and a new expression can be found which include the yaw control and its associated error. It can be written as

$$P = \frac{1}{2} C_p \rho A_{swept} v^3 cos(\theta), \tag{2.5}$$

and is the modified wind power equation [33], [34].

2.4 Wave Power

Water covers about 71 percent of the worlds surface area and have a huge energy potential [36]. From a report which the World Energy Council presented 2010, they estimated the potential energy, which could be generated from wave harvesting to be 32 $PWh/year$ [37]. This is approximately twice of the global energy production 2008. Improvements of wave power regarding construction and efficiency have been made during past years and together with the potential, interest regarding the technology have increased [38].

A wave power plant can utilize different technologies, but all use the wave's potential and kinetic energy, or either of them, to generate power [38]. Wave power plants are designed to generate large amounts of energy and to handle the external forces which it is subjected to, the plant is therefore required to be of large size. As the plant is located at the sea, area requirements are of less concern. Instead, the plant can be immobile and ill-shaped for transportation. Installation cost is high and logistic associated with wave power plants can be complicated, the installation therefore need to be of high power to be economically beneficial.

2.5 Energy Storage System

As described in section 2.1, the designed off-grid harvesting system produce energy from renewable energy sources. The power outputs from renewable energy sources are essentially variable due to the intermittent characteristics of the weather. Without an ESS, enough energy need to be produced to meet the demand at every instant to maintain a continuous operation for the radar. Produced energy which exceeds the required demand will be dissipated as losses, as there is no place to store the energy. ESSs are therefore required in an energy harvesting system to maintain a continuous operation and to help minimize losses due to over production.

For an ESS, different technologies and typologies can be utilized. Depending on the requirements and environment, some technologies are more interesting compared to other. For operation in an off-grid harvesting system, well documented technologies are Lead acid-, Lithium-ion batteries and hydrogen storage.

2.5.1 Lithium-ion Batteries

Lithium-ion batteries (LiBs) are the ion batteries with the highest specific capacity [Ah/kg]. This is due to the small atom- weight and radius of Lithium [39]. LiBs are used in applications where size and weight are of importance, such as smartphones[3] and electric buses[4]. There are various types of LiBs, and each type is based upon different Li-polymers. Lithium Nickel Manganese Cobalt Oxide (NMC) batteries have a high specific capacity while Lithium Iron Phosphate (LFP) batteries are more robust and more thermally stable [39].

The downside of LiBs are mainly sustainable aspects. The accessibility of Lithium, Cobolt, Nickel and Graphite is limited and with increasing demand, the cost also increased. The main suppliers of these materials are a few countries which the market is fully dependent on. Projections regarding the Lithium accessibility, which come from the electrical vehicle industry, predict an increase in demand of batteries and it also mention that by 2025, the global Lithium supply will be depleted [40].

Substances in LiBs, specifically Cobalt, is poisonous in too high concentrations and humans should avoid being exposed to it. Because of the mining and the management, it may damage the environment and humans in the surrounding [41]. Through Cobalt mining, the health of many humans have been affected in a negative way and the mining procedure have also been related to child labor [42].

2.5.2 Lead Acid Batteries

Today's battery market is mainly based upon lead acid batteries. It was one of the most advanced battery technologies for a long period of time and have a high

[3]https://support.apple.com/kb/SP770?locale=en_GB, D.O.A 2019:05:21

[4]https://www.volvobuses.co.uk/en-gb/our-offering/buses/volvo-7900-electric/specifications.html, D.O.A 2019:05:21

power capacity, is relatively cheap and is easy to manufacture [43]. Lead acid have an high theoretical specific energy of $171Wh/kg$. In reality the battery only have a specific energy of 25-40Wh/kg due to its high water content, which is used for its electrochemical reaction [43]. The efficiency of lead acid batteries is lower than LiBs, but it is close to 100% at low powers [44].

2.5.3 Supercapacitors

Supercapacitors are electrochemical capacitors which can be used as energy storage systems. Electrochemical capacitors are divided into different subgroups, where the electrical double layer capacitor (EDLC) is the most advanced technology at the moment [45].

The strength of supercapacitors is its power density, where supercapacitors are dominant compared to batteries. Instead, the downside is its energy density, which is low. With these properties, the cycles could be more frequent, but fortunately supercapacitors have much higher cycle life and life length compared to batteries [45].

Unlike batteries, which can have a rather flat voltage discharge curve, supercapacitors voltage change more. The voltage change follow the capacitance equation,

$$i(t) = C\frac{dv(t)}{dt},$$

which makes it proportional to the charged/discharged current and the voltage-SOC curve is a straight line. This makes estimations regarding the state of charge (SOC) of the capacitor easier, but in applications where a stable voltage is required, additional converters are needed.

2.5.4 Aging and Comparison of Batteries

The life length of a battery is difficult to estimate and it can be prolonged or shortened by the operation point. Factors such as operating temperature, charge- and discharge current and depth of discharge (DOD) have a significant impact on the life length [46], [47]. Also, the storage of the battery when not used will affect the aging [46], [47]. When batteries age, the usable capacity decrease and the internal resistance increase. This is due to side reactions, which change the structure of active materials in the electrodes and add material layers on top of them [46]–[48]. Different batteries age differently, even if they are of the same design, which make estimations difficult to make, but from measurements, predictions and models can be made.

Lead acid batteries are more sensitive to temperatures than LiBs, and temperatures over 25°C have a larger impact on lead acid batteries. For temperatures between 0-20°C, the impact of aging is almost neglectable, but at these temperatures the internal resistance changes [44], [49]. The general cycle life for LiBs are longer than

for Lead acid batteries and this is presented in table 2.3.

To keep the battery temperature at a steady level, one solution is to bury the battery in the ground. Since the thermal conductivity in the ground is low, the temperature varies less. With the Kusuda-Achenbach model [50], a valid estimation of the temperature in Gothenburg at different depth in the ground can be made, which can be seen in figure 2.7. At a depth of 4m, the temperature of the battery will never fall below 0°C.

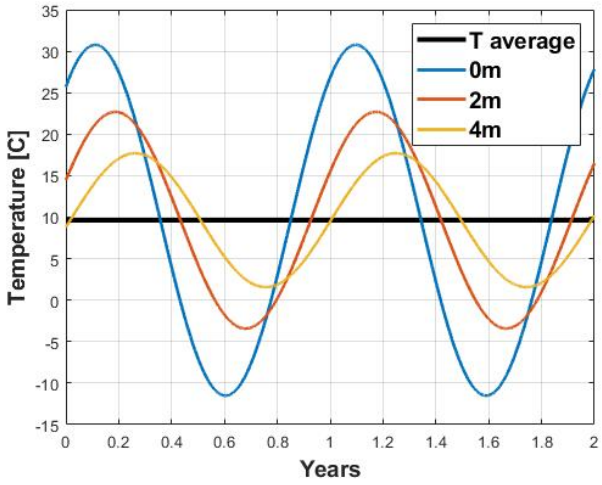

Figure 2.7: How the average temperature change over several years at different depth in the ground.

To aid the decision of which ESS is the most suitable for a given application, table 2.3 was compiled. The comparison is done with NMC LiBs, as it display the necessary differences between Lead Acid batteries and LiBs. The values which is displayed in table 2.3 are from battery packs, which is different from the theoretical values. This mean that casing and other protection is added into the weight.

Table 2.3: Comparison between supercapacitors, lead acid and lithium-ion on a pack level.

	Supercapacitor [45][51]	Lead Acid [44]	Lithium-ion [44]
Specific capacity $[Wh/kg]$	1-10	40	150
Specific Power $[W/kg]$	500-10,000	1,000	512
Efficiency [%]			
@ 0.05C	100	100	100
@ 0.25C	100	80	99
@ 1C	100	60	92
Cycle Life	Millions	1,000 @50% DoD	1,900 @80% DoD
Initial Cost $[\$/kWh]$	300–2000[52]	70[5]-120	120[6]-600
Temperature Sensitivity	-	Degrades significantly above 25°C	Degrades significantly above 45°C

2.5.5 Hydrogen Storage

After some alterations, today's combustion engines can operate with hydrogen, and the transition from fossil to hydrogen could potentially be easier than to electric motors. Unlike fossil fuels, the by-product of using hydrogen is H_2O instead of carbon oxides. The principle of hydrogen storage is to store and use hydrogen in fuel cells, which are used to generate electricity in a closed chemical system. In comparison to batteries, the amount of energy which can be stored is very large. This is because hydrogen is stored in high pressure tanks. Continuing the comparison, the efficiency of fuel cells are poor and do not reach more than 30%, assumed that the heat losses cannot be utilized [53].

As mentioned in section 1.1, there is a household in Agnesberg, Gothenburg that use only sustainable energy sources. The household utilize hydrogen to supply his house with power and heat during the winter. When his battery pack is fully charged, the excess power produced is used in the electrolysis process to produce hydrogen [53]. Hydrogen storage is like battery storage, a proven alternative for ESS but due to its low efficiency, it would require a larger system.

[5]https://www.alibaba.com/product-detail/Yangtze-solar-Lead-acid-gel-battery_62111813501.html?spm=a2700.7724838.2017115.27.5b4f7d60H6Ttb7&s=p, D.O.A: 2019:05:16

[6]https://www.alibaba.com/product-detail/rechargeable-lithium-ion-prismatic-cells-3_62001367650.html?spm=a2700.7724838.2017115.32.210f37139vRyWl&s=p, D.O.A: 2019:05:16

2.6 Power Electronics

To ensure that the radar system is kept at the rated voltage, electrical power converters are needed. Depending on the application and if galvanic isolation is needed, different designs are of interest. Ideal components are assumed to simplify the equations for the converters. This include that no components have an equivalent series resistance (ESR), that switches do not have a commutation time or losses and that diodes do not have any voltage drop.

Design of components are done under continuous conduction mode (CCM) and steady-state operation. To ensure that the converter is operating in CCM, the following expression,

$$I_L - \frac{\Delta i_L}{2} > 0, \tag{2.6}$$

need to be true over the entire operation range. From (2.6), I_L represent the average current which flow through the inductor and Δi_L is the peak-peak ripple of the inductor current.

2.6.1 Step-down (Buck) Converter

A buck converter distribute power from the high voltage side to the low voltage side. Figure 2.8 show the topology of a buck converter and that a switch, a diode, a capacitor and an inductor is included. Depending on the on-time, t_{on}, of the switch, it is possible to change the voltage on the low voltage side. The transfer function for the buck converter is,

$$\frac{V_o}{V_d} = D, \tag{2.7}$$

where D represent the duty cycle of the switch and is a ratio between the on-time and the switching period, T_s. V_o is the output voltage and last, V_d is the high voltage side and also the input. From (2.7) it is noticed that the duty cycle is proportional to the ratio of the low- and high voltage side. To be able to keep the voltage constant at the low voltage side, a controller can be implemented. A controller method which is commonly used is pulse-width modulation (PWM) and is connected to the switch to control the duty cycle.

The components, essentially the inductor and the capacitor are to be designed to meet the requirements. The inductor is related to the current ripple and the capacitor to the voltage ripple. How the inductor relate to the output ripple can be expressed accordingly to,

$$\Delta i_L = \frac{V_o}{L}(1 - D)T_s, \tag{2.8}$$

where L is the inductance. From (2.8) it can be seen that CCM is ensured as long as the current ripple is designed as a percentage of the current which flow though the inductor. The inductor value is to be chosen to ensure that the current ripple

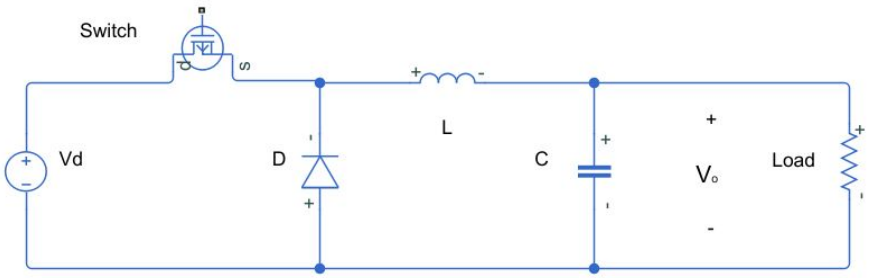

Figure 2.8: Display how a buck converter can be designed and the essential components which it consists of.

percentage is lesser than 50%, otherwise operation in CCM can not be guaranteed at all times. As for the capacitor, it is chosen depending on the allowed voltage ripple and how the capacitor relate to the output voltage ripple is,

$$\Delta V_o = \frac{\Delta Q}{C} = \frac{\Delta I_L T_s}{8C}, \tag{2.9}$$

where, Q is the stored energy in the capacitor and C represent the capacitance [54]. From (2.8) and (2.9), the relationship of how the components relate to the ripple can be seen and from there, and depending on the requirements regarding ripple, values for the components can be calculated.

2.6.2 Step-up (Boost) Converter

For the boost converter, the power is transferred from the low voltage side to the high voltage side and to accomplish this, the topology which can be seen in figure 2.9 is utilized.

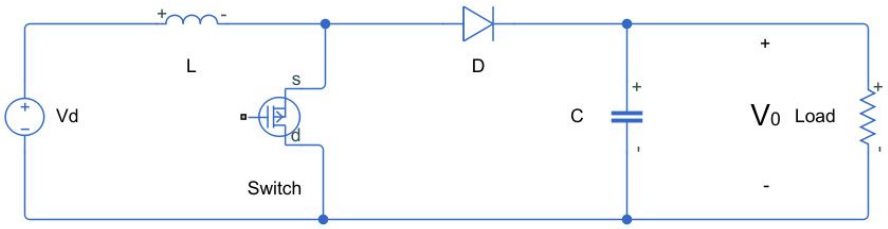

Figure 2.9: Display how a boost converter can be designed and what components that are needed.

The transfer function for the boost converter, if operation in CCM is assumed, can be expressed as,

$$\frac{V_o}{V_d} = \frac{1}{1-D}, \tag{2.10}$$

and it can be noticed that the higher the duty cycle, the higher the ratio between the input and output voltage is. With the same principle as explained in section 2.6.1, a controller can help to ensure that the output voltage is kept at a constant

level. To meet requirements regarding ripple, the components need to be sized. The capacitor is related to the output voltage and can be sized in the following way [54],

$$\Delta V_o = \frac{\Delta Q}{C} = \frac{I_o D T_s}{C} \tag{2.11}$$

Depending on the ripple factor, the capacitance can be calculated from (2.11). To keep the ripple current suppressed and to ensure operation in CCM, the inductor need to be designed. If the current drops too low, the converter starts to operate in discontinuous conduction mode (DCM). This boundary limit for the inductor current, I_{LB}, can be expressed as,

$$I_{LB} = \frac{1}{2}\Delta i_L = \frac{T_s V_o}{2L} D(1-D) \tag{2.12}$$

This can be rewritten as an expression of the inductance, which depends on the output boundary current, I_{oB}, which is the minimum current the converter can supply the with output in CCM operation. The inductance can be expressed as,

$$L = \frac{T_s V_o}{2 I_{oB}} D(1-D)^2 \tag{2.13}$$

With (2.11) and (2.13), the boost converters inductor and capacitor can be designed with predetermined voltage- levels, ripple and boundary current.

2.6.3 Bidirectional Converter

In an ESS there is a need to transfer power in both directions, when charging and discharging the storage [55], [56]. Figure 2.10 display a bidirectional converter which can act as a buck converter in one way and a boost in the other direction. While in buck mode, switch $S1$ is closed, while $S2$ is switching and vice verse for boost mode. By controlling the switches $S1$ and $S2$, power can be transferred in both directions and it is possible to charge and discharge the ESS.

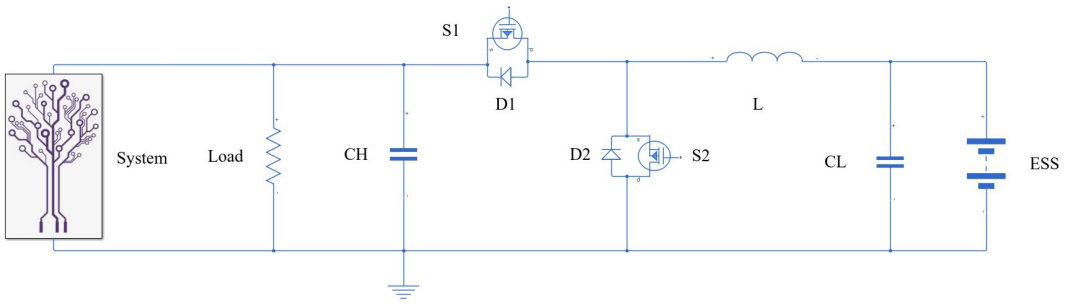

Figure 2.10: Design of a bidirectional DC/DC converter.

2.6.4 Flyback Converter

A conventionally used buck-boost converter is the flyback converter. It have the characteristics of both the buck- and the boost converter and can increase or decrease the output voltage depending on the duty cycle. The transfer function when operating in CCM is expressed as,

$$\frac{V_o}{V_d} = \frac{N_3}{N_1}\frac{D}{1-D}, \tag{2.14}$$

and from (2.14) it can be noted that a flyback converter can act as a buck converter during certain duty cycles and as a boost converter during other. Specific intervals can be found in the case that the number of transformer windings are know. A difference for the flyback converter compared to prior mentioned converters is that it includes galvanic isolation, due to the included transformers. The transformers can be noted in figure 2.11. The presented flyback design includes three transformer windings, where N_1 is for the primary side, N_3 for the secondary side and the last for voltage protection, N_2 is included. The protection limit the output voltage to a certain value depending on the number of windings on N_2 and N_3.

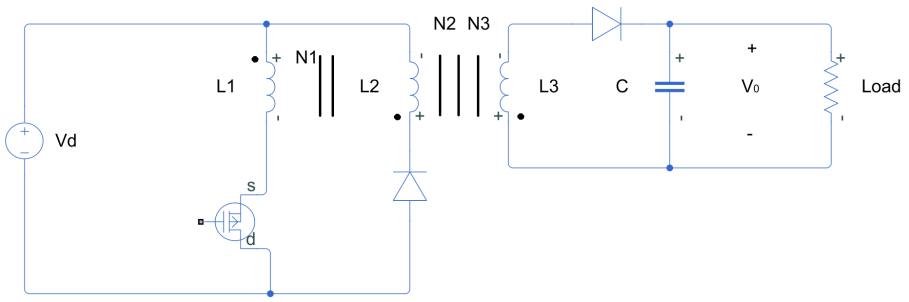

Figure 2.11: How a flyback converter may look like. Necessary components such as capacitors and inductors are included.

To ensure operation in CCM, sizing of the magnetizing inductor in the transformer is needed. By using figure 2.11 and analyzing the circuit, it is possible to notice that,

$$I_m = I_d + I_o\frac{N_3}{N_1},$$

where I_m is the magnetizing current for the transformer at the primary side, N_1. By substitution and rearrangement, an expression for the magnetizing inductor can be found. It follows,

$$\frac{V_o Io}{V_d} + \frac{V_o}{R_{Load}}\frac{N_3}{N_1} > \frac{DV_d T_s}{2L_m}, \tag{2.15}$$

and, by choosing L_m the converter can ensure operation in CCM.

2.7 Snubbers

In electronic circuits which consist of switches, there will be losses associated with the switch. To reduce the losses and stress related of switching, snubbers are used. A snubber is able to limit the voltage overshoot of a semiconductor during its turn-off period and limit the rate of change in the voltage across the semiconductor under the turn-off period. It can also limit the current through the semiconductor, shape the switching trajectory and limit the rate of rise of the current through the semiconductor during the turn-on period [54].

In the presented converters there is a need to use two different semiconductors, a diode and a switch. A snubber for the diode, and one for the switch is therefore implemented. The design of the diode snubber and that of the switching snubber is different and will thus be separated and presented individually.

2.7.1 Diode Snubbers

A diode snubber is mainly used to limit overvoltage over the diode. A possible design of a diode snubber is presented in figure 2.12, and it can be seen that it consists of a resistance and a capacitance connected in series. The two components are connected in parallel with the diode. An stray inductance, L_σ, is also included to make the system more realistic.

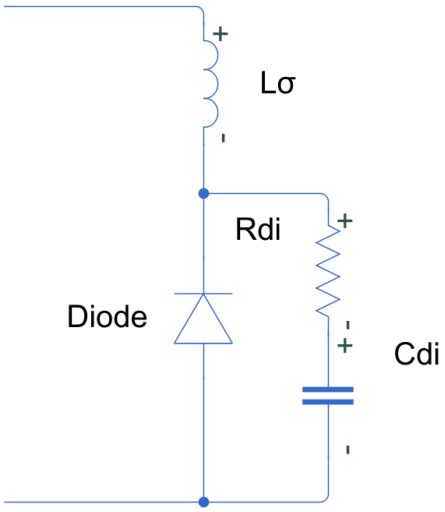

Figure 2.12: Display how a diode snubber may look like.

The component value for the resistance, R_{di}, and the capacitance, C_{di}, can be calculated depending on the waveform of the current and the voltage. The value of the stray inductance is also of importance when the values of the components are chosen. The base resistance, R_{base}, for the resistance in the diode snubber can be calculated according to

$$R_{base} = \frac{V_d}{I_{rr}}, \tag{2.16}$$

and from (2.16), V_d is the forward voltage over the diode and I_{rr} is the reverse recovery current. The value for the resistance, R_{di}, should be chosen as a value larger than R_{base}. According to [54], the optimal value for the resistance is when $R_{di} = 1.3R_{base}$, under the condition that the capacitance is selected as its base value. The base value for the capacitance, C_{base}, can be calculated as

$$C_{base} = L_\sigma \frac{I_{rr}}{V_d}^2 \tag{2.17}$$

2.7.2 Switch Snubbers

Two types of switch snubbers are turn-off and turn-on snubbers. For converters, the turn-off period is a major problem and is related to large losses [54]. To limit the power loss, a turn-off snubber is used and in figure 2.13a a possible design of a turn-off snubber is displayed. From figure 2.13a, similarities to a diode snubber can be seen, but the turn-off switch snubber includes a diode which is connected parallel to the resistance.

For the resistance, R_{sw}, and the capacitance, C_{sw}, their values can be calculated by observing the waveform of the current and voltage during a switching event. By using the waveforms, the rise time of the current t_{fi}, the stabilized value for the current I_o and the voltage, V_d, over the switch can be found. With this information, it is possible to calculate the capacitance according to

$$C_{sw} = \frac{I_0 t_{fi}}{2V_d} \tag{2.18}$$

The resistance of the snubber can be calculated in the following way,

$$R_{sw} > \frac{V_d}{I_{rr}}, \tag{2.19}$$

where R_{sw} based upon the desired protection and the selected loss minimization criterias.

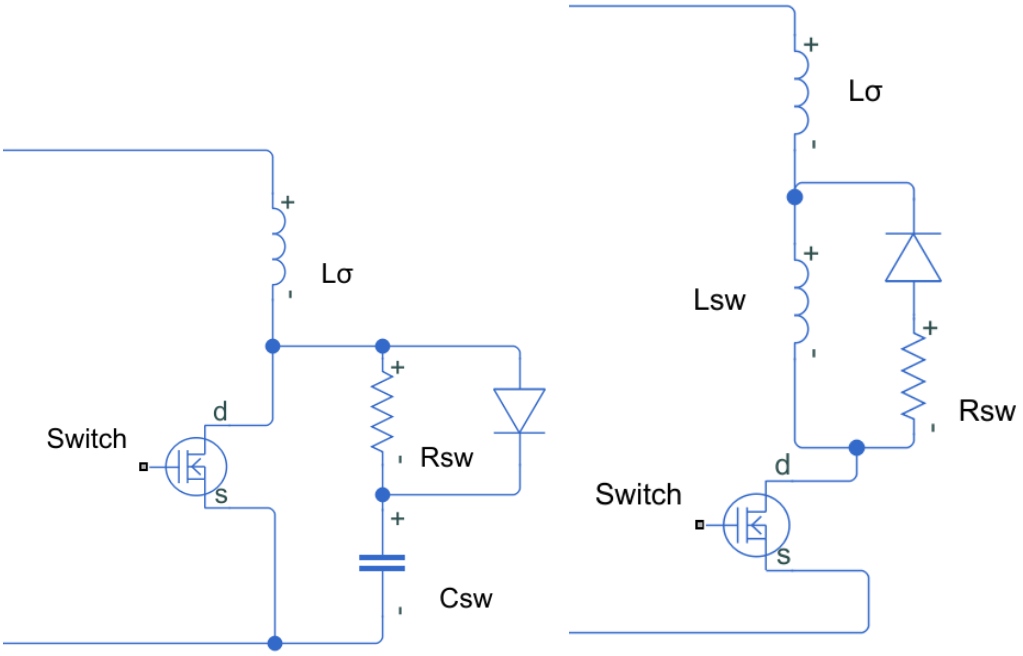

(a) Display how a turn-off snubber may look like.

(b) Display the design of a turn-on snubber.

Figure 2.13: Switch snubbers

As for the second switch snubber, the turn-on snubber, it is dissimilar with the other presented snubbers because it is connected in series with the semiconductor instead of parallel. The design for a turn-on snubber is presented in figure 2.13b. Additionally, the turn-on snubber have an inductance, L_{sw}, instead of a capacitance. The inductance can be calculated accordingly to,

$$L_{sw} = \frac{\Delta V_{ds} t_{ri}}{I_0}, \tag{2.20}$$

where ΔV_{ds} is the transistor's overvoltage at a turn-on event and t_{ri} is the rise time of the current. The resistance can be designed such that it let the inductor current decrease to a low value before the next turn-on event, which is done by investigating the current waveforms and tuning the resistance.

3
The Radar

The radar, which the system should provide energy for, is described in this chapter. It does not always have to operate in the same way and therefore this chapter describes two modes of operation.

In table 3.1 the prerequisites of the radar are presented. From table 3.1, a voltage level of $54V$ is selected as the supply voltage. The power electronic in the system is design to maintain these specifications with a margin to secure safe operation. The maximum peak-peak voltage ripple is used when selecting the power electronic ripple, and it is design to manage this limit with a great margin.

Table 3.1: Prerequisites for the radar

Nominal supply voltage	$54V DC \pm 1V$
Normal supply voltage	46-62VDC
Maximum output power estimated	260W
Maximum peak-peak voltage ripple	$2.5V$

3.1 Continuous Operation

The first mode of operation is continuous operation. In this operation, the radar is transmitting and receiving data at all times and have a continuous power demand of $260W$, which is the estimated maximum output power, see table 3.1. This is the operation which have the highest power demand and therefore the largest system is sized to meet this demand.

3.2 Interval Operation

The operation does not necessary need to be continuous operation but could be of an interval operation. The second operation mode investigated is interval operation, with a period time of five seconds and a duty cycle of 20%, as can be seen in figure 3.1. By transmitting for one second, a good accuracy can be obtained, and waiting for no more then four seconds do not let targets to move far without being detected. In reality, if a target have been detected, the duty cycle may change to be able to follow the object of interest. When not transmitting there is a stand-by power which is set to $30W$. This power represent the internal data processing and communication

link. The average power of the interval operation is $82W$. This would decrease the system sizes, as lesser amount of energy need to be generated.

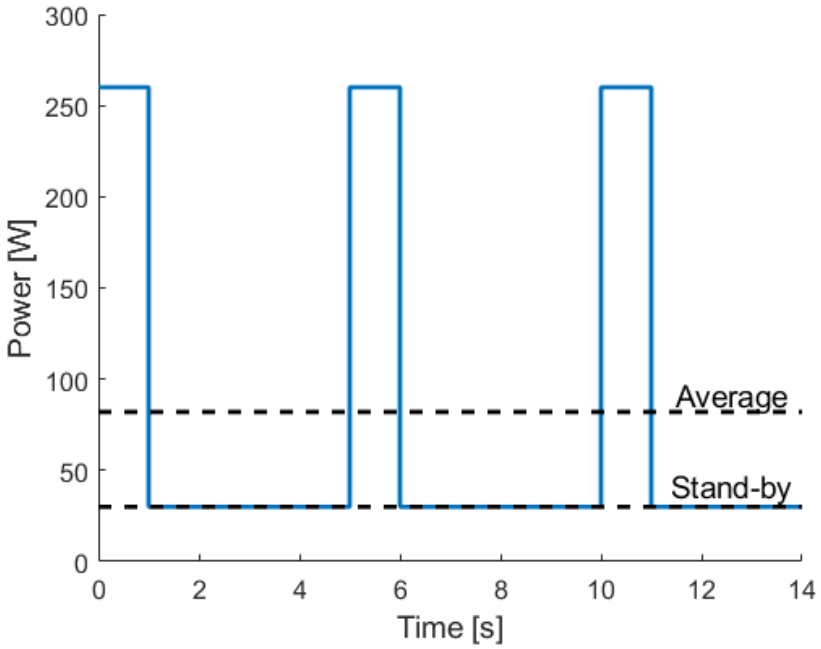

Figure 3.1: Radar input power during interval operation.

4

Energy System Modulation

In this chapter, argumentation and reasoning which is related to the final system will be presented. Comparisons between different renewable energy sources are to be conducted, to motivate the use of certain technologies. Additionally, the design of the ESS will be presented to be able to generate a complete model of the system.

To generate sufficiently with energy for the radar, different renewable energy sources can be utilized and three alternatives have previously been mentioned, solar-, wind- and wave power. For the given requirements, a small generating system is needed, which is compact and is able to produce enough energy at the given location. As mentioned in section 2.4, wave power generators are usually of larger size, higher power rating and located at the seabed. This limits the potential radar placement to near coastlines, which may not be desirable. With solar- or wind power, additional locations will be available for the radar compared to using wave power. As small scale wave power plants are close to non-existing and due to the limiting placements, wave power have been decided to not be a suitable generating source for this application.

Depending on the selected location and environment, solar- and wind power generation can be suitable sources of energy. Both technologies can be expanded and be sized depending on the specific power level. As the systems can be sized depending on the environmental surroundings and the required power, the system can be sized to be as compact as possible. Hence, solar- and wind power generation have been chosen as suitable energy sources for the application. Two models will therefore be used, one for the wind- and one for the solar- power generation. For different locations, adjustments regarding sizing will be done based on available weather data. As the system is connected to an ESS, readjustment need to be done with respect to the capacity of the storage so the system is kept as compact as possible while keeping the cost low.

4.1 Weather Data Acquirement

`SMHI` collects data from weather stations all over Sweden, which is available free of charge on its web page[7]. The weather data for Gothenburg used is taken from this source and the acquired solar- and wind data is an average value for each hour. Solar data is given in irradiation $[W/m^2]$ and wind speed in velocity $[m/s]$ for the

[7]https://www.smhi.se/klimatdata, D.O.A: 2019:05:16

wind data. For the second and third location, Sde Boker and Thule, the data was taken from `NASA`[8] and `Iowa State University`[9] respectively.

During certain periods, the data acquired were missing measurements. This was solved by manually filling in suitable values based upon neighboring data from the location. The weather data is shown in figure 4.1, 4.2 and 4.3, which includes temperature, wind speed and solar radiation. The temperature is lower at locations at higher latitudes. A similar correlation with the radiation can be noticed and the sun shines more evenly over the year closer to the equator and the radiation is relatively high the year around in Sde Boker. Gothenburg is the windiest location out of the three.

[8]https://solrad-net.gsfc.nasa.gov/, D.O.A: 2019:05:16

[9]https://mesonet.agron.iastate.edu/request/download.phtml?network=IL___ASOS, D.O.A: 2019:05:16

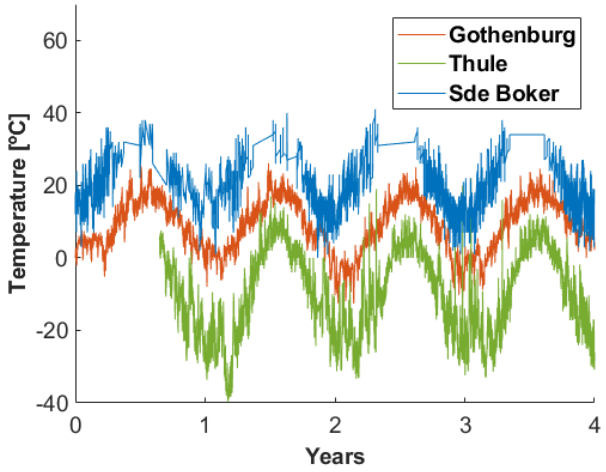

	Average [°C]	Min [°C]	Max [°C]
Gothenburg	8.6	-12.6	26.1
Sde Boker	23.6	0.0	41.0
Thule	-9.7	-39.7	22.0

Figure 4.1: Temperature for each location including average, minimum and maximum value.

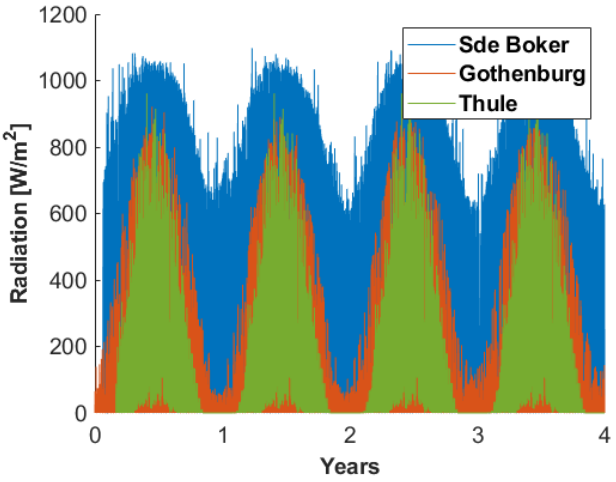

	Average [W/m^2]
Gothenburg	111
Sde Boker	244
Thule	104

Figure 4.2: Irradiation for each location including the average value.

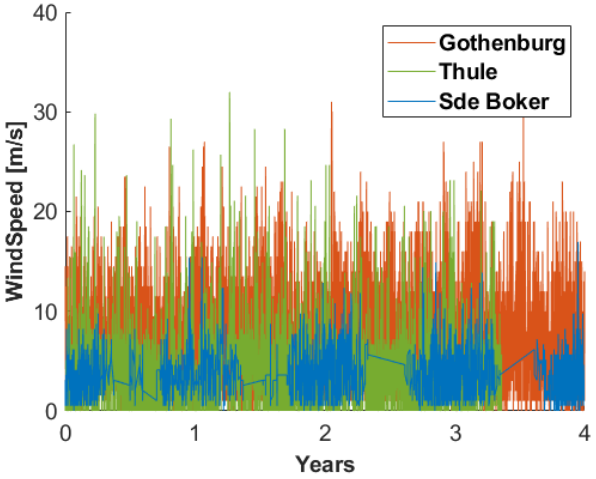

	Average [m/s]	Standard Deviation
Gothenburg	7.4	4.0
Sde Boker	3.8	2.4
Thule	4.3	4.3

Figure 4.3: Wind velocity at each locations including average value and standard deviation.

4.2 Solar Energy Model

For the solar model, it can use either a PV or a CSP based topology. The required power rating and area requirement are the deciding factors in the decision of which technology that is the most suitable. CSP technologies require larger space compared to a PV system and need to be of larger size to be able to archive a higher efficiency. As for a PV system, it can be designed to have a high efficiency for the required power rating. Therefore, the model will be based on a PV system.

The PV system will be based on mono crystalline silicon as this technology has the highest efficiency compared to other mentioned technologies, see table 2.1. The cost of the system increase due to the use of mono crystalline cells, but the area or number of PV cells will be reduced as a result of the higher efficiency. After evaluating the trade-off between area occupation and initial cost, the mono crystalline design was found to be preferable to use.

To be able to generate a model from a product sheet: two assumptions have been made regarding the solar cell model. The first assumption is that a MPPT is not designed in the project, instead a quasi-MPPT is used and it is assumed to give the maximum power point at each instant. From experimental results, shown in appendix A, it can be seen that the same relationship which is presented regarding V_{oc} and I_{sc} can be applied for the maximum power point too. An error in the range of 6% can be noted due to the assumption, except for two data points.

The second assumption is that the temperature dependence which exists for V_{oc} and I_{sc} can be applied to the maximum power point for the PV system. The error which is associated with the temperature dependence have a minimal impact compared to the previously mentioned error and, hence can this assumption be made.

4.2.1 Choice of PV Cells

The PV model is based upon data from $NOCT$ conditions and therefore, only manufacturers which present this information are considered. A PV cell from Solar World[10] with a size of $1.67m^2$, was chosen, and the model is generated to mimic the same behaviour as the chosen PV cell. How the power output of the model change with the irradiation can be seen in figure 4.4 and an almost proportional relationship is seen. The product can be bought for $210 in a retail store. The cell have its maximum power point at a voltage of $29.5V$ and a current of $7.43A$ at $NOCT$ conditions, which result in a power output of $219.2W$.

The complete model use a PV cell configuration to achieve a specific voltage and/or power level. The voltage level of the PV cells should be designed to always be lesser or greater than the radar voltage regardless of the irradiation and the temperature. It have therefore been decided to keep a minimum of three cells in series which gives

[10]https://www.solaris-shop.com/solarworld-swa-290-plus-290w-mono-solar-panel/ D.O.A: 2019:05:21

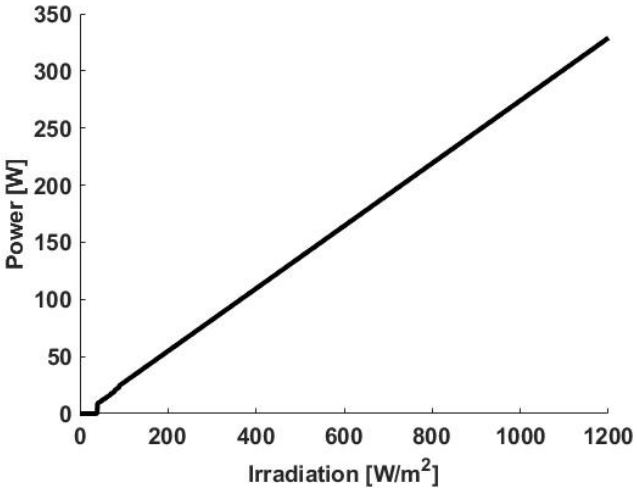

Figure 4.4: Display how the power output from a single PV cell change with irradiation. Temperature is set as $300K$.

an voltage of around $88.5V$. As for the number of parallel connected PV cells, it is dependent on the required power demand and the environmental surrounding.

4.3 Wind Power Model

The designed wind power model is compatible with both vertical and horizontal turbines where the VAWT uses (2.4) and HAWT follows (2.5). Additionally, a cut-in-, cut-out- and cut-off-speed is implemented to know at which wind speed the turbine can start to generate power, reach maximum generation and terminate the production. The maximum power coefficient, C_p, will increase to its rated value after the speed exceeds the cut-in-speed and decrease at its cut-out-speed.

Two products, one VAWT[11] and one HAWT[12] have been selected to be used and their power curve from the model can be seen in figure 4.5. The previously mentioned parameters can be seen in table 4.1 and relate to the selected HAWT and VAWT.

These two turbines have desired power ratings and an output voltage of 48V. The parameters which are used in the model are based on the selected product specifications. The selected HAWT have an initial cost of \$300[12] and requires a minimum of $3m^2$ of area. Additionally, the VAWT have an initial cost of around \$250[11] and have a area requirement of $1m^2$.

[11]https://www.alibaba.com/product-detail/Vertical-axis-wind-turbine_60733877884.html?spm=a2700.7724838.2017115.34.4be04065Ouz9PRs=p, D.O.A: 2019:05:16

[12]https://www.alibaba.com/product-detail/Chinese-Complete-Home-System-3-Phase_60843504166.html?spm=a2700.7724838.2017115.117.4be04065Ouz9PRs=p, D.O.A: 2019:05:16

Table 4.1: Wind speed parameters for the horizontal- and vertical wind turbines.

	Cut-in speed $[m/s]$	Cut-out speed $[m/s]$	Cut-off speed $[m/s]$
HAWT	2	12.5	45
VAWT	2	11	45

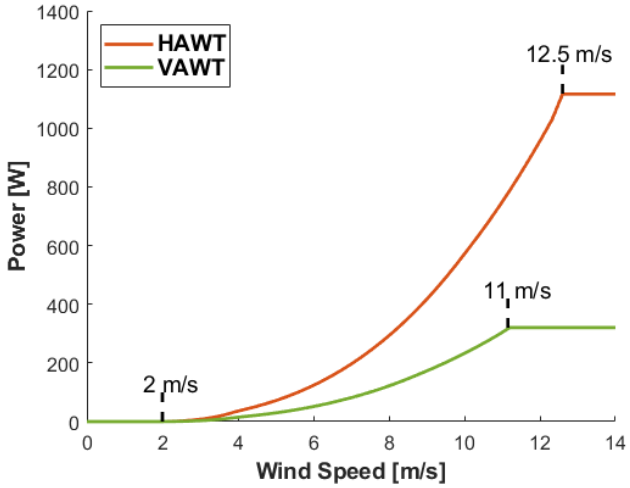

Figure 4.5: The power output from the two wind turbines at different wind speeds.

4.4 Battery Model

If a storage system with high- efficiency and energy capacity is of interest, then a battery is a proven choice which is selected for this model. The battery is modeled as a voltage source in series with an internal resistance, as shown in figure 4.6. Neither of these components are constant but are described as functions of the SOC and the temperature of the battery. If the battery was simply modeled as only a voltage source, the losses would not be included and more advanced models than the proposed model are mainly used when the frequency response of the battery is of importance. The internal resistance will generate a power loss and a voltage drop in the battery.

LiBs are chosen over lead acid batteries and supercapacitors due to their high energy density. LiBs also have longer cycle life and are more stable in a wider temperature range. Even though the cost of LiBs are higher, the pros weighs up for it. Regarding the temperature, LFP is a LiB type with rather good tolerance. Additionally, other LiB types, such as NMC, consists of metals like Cobalt and Manganese. From an sustainable aspect LFP is to be preferred.

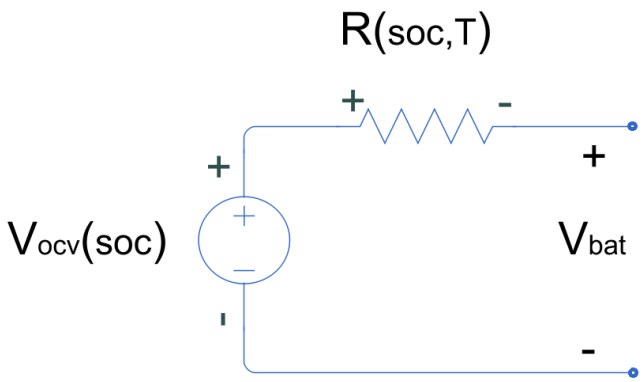

Figure 4.6: The battery model.

The V_{ocv}-SOC curve is taken from measurements of a LFP coin cell and the modeling of internal resistance is done from measurements in [49]. Both of these measurements are shown in figure 4.7. A SOC window is used which means that the battery never gets fully discharged nor fully charged. This window is set as 20%-90%. Battery cells are connected in series and parallel to achieve the required energy capacities and voltage level. A voltage level of $48V$ was selected for the battery.

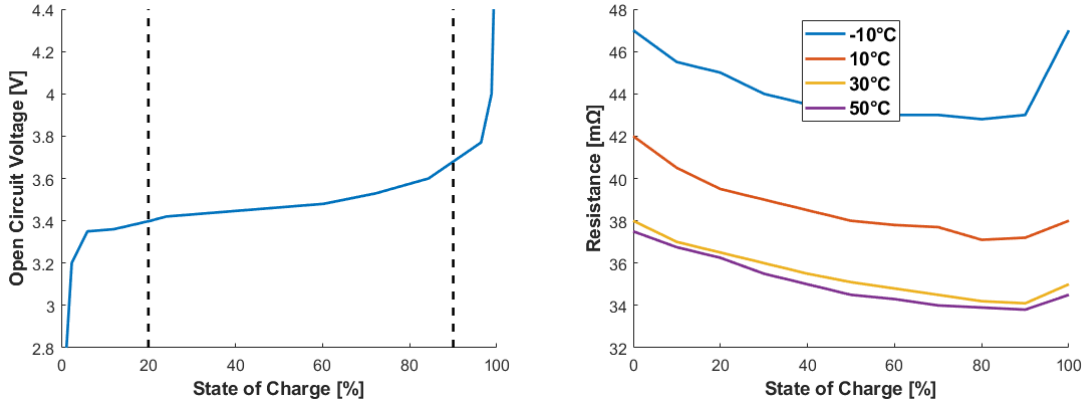

(a) V_{ocv}-SOC curve of a LFP cell.

(b) Resistance of a LFP cell at different temperatures and SOC levels.

Figure 4.7: The measurements which the battery model is based upon.

Comparing the amount of current which flow into the battery with the discharge current, a net current can be calculated. Integrating this net current and comparing it with the battery capacity, the battery's SOC can be calculated and visualized. The current into the battery is set to zero if the battery is fully charged and if the battery is depleted at anytime, the system is undersized. Thus, by observing the SOC of the battery during simulation, sizing of the battery can be carried out. Due to uncertainties and the complexity of aging in batteries, this is not implemented in the model. Although, the aging is taken into consideration by adding 25% extra energy capacity to the calculated value. This is done in order to secure a safe and long operation life for the battery.

5
Converter Design

For the system, there will be a need of a maximum of three converters: one connected to the solar PV cells, one to the wind turbine and lastly, one at the battery. Each of the mentioned converters have different purposes and therefore each converter has different requirements to meet. Similar for each converter is that they need to include safety marginals. The marginals help to ensure operation in CCM, as mentioned in section 2.6, and to limit faults.

By comparing the voltage levels at each connection, a conclusion regrading the necessary converter design can be made. For the two converters connected to the power sources, they will have the same output voltage, which is the DC voltage that the radar requires. The input voltage for these two converters are dependent on the output from the power source and vary from product to product. As mentioned in section 4.3, the chosen wind turbines have an output voltage of $48V$. A boost or a flyback topology can be used for the application, but a flyback converter is mainly used in circuits where the high voltage is present. It is therefore decided to use and boost converter as it generally have a higher efficiency.

In section 4.2.1 it was mentioned that the output voltage of the PV system were designed to $88.5V$. By comparing the PV voltage with the required voltage at the radar, which is $54V$, a clear disparity is seen. Due to this, a flyback or a buck converter topology can be used. The main reason to use a flyback converter is because of the galvanic isolation and protection it provided. For the PV system, high efficiency is of high importance and additional protection can be provided through relays, thus it was decided that there is no need to use a flyback converter. Therefore, a buck converter have been chosen.

For the converter connected to the ESS, it will use the bidirectional topology, due to the need to transport power in both directions. The converter will be designed in two steps, one for each direction. It acts as a boost converter in one direction, using the boost topology which have been presented and for the opposite direction, the buck topology will be used instead.

When calculating the components values, a switching frequency must be chosen. A switching frequency of $500kHz$ have been chosen and is mainly chosen as a high value to help to minimize the size of the components. Other frequencies can be chosen, but $500kHz$ is a standardized value and there exist components which use this frequency. It have therefore been chosen as the switching frequency for all the

converters in the system. Additionally, it is required to know the maximum amount of current which will flow through the converters. This is done in order to ensure that the components can be chosen accordingly.

The output voltage of each converter include ripple due to the switching in the circuit. The ripple is desired to be minimized as the output is a DC voltage. To secure a low ripple, the ripple voltage have been designed as 1% of the output voltage. This is also to ensure that the voltage which the radar is supplied with is kept within the requirements. By using 1% of the output voltage as a guideline for the ripple, it should be kept within limits with marginal.

5.1 Buck Converter Design

For the PV system, because the number of parallel solar cells are decided based upon the required power production, it is unknown what amount of current that will flow through the converter. It have therefore been decided to allow a maximum current of around $25A$ which represent a current from a $3x3$ cell configuration. Additionally, to ensure operation in CCM at most times, a minimum current ripple, Δi_L, of $0.3A$ was selected.

The buck converter's inductance and capacitance are calculated with the use of (2.8) and (2.9) respectively. By including non-ideal components, the calculated values may not be the best solution as the equations are besed upon ideal conditions. The components values are therefore changed through trial-and-error to find a better solution.

5.2 Boost Converter Design

The wind boost converters are designed to fit the horizontal-axis wind turbine and an input voltage of $48V$, as presented in section 4.3. Similar to the PV buck converter, the output voltage is $54V$. The maximum power output of the wind turbine is $1100W$, which results in a maximum current of $21A$. For the output boundary current, I_{oB}, it is selected to be $0.3A$.

With (2.11) and (2.13), the boost converters inductance and capacitance are calculated. Afterwards, the components could be chosen with considerations to the parasitic elements and re-selected.

5.3 Bidirectional Converter Design

For the design of the bidirectional converter, both the power directions are taken into consideration. The low voltage side of the converter is the battery side with a voltage level of $48V$ and the high voltage side is the radar, with a voltage of $54V$. When discharging the battery, the output current will not exceed $4.8A$, as this is the

required current the radar require during rated operation conditions. In the case of charging, the maximum allowed current is set with regards to the power production limits according to

$$I_{max,Solar} + I_{max,Wind,max} - I_{radar} = I_{Battery,max},$$

$$25A + 21A - 4.8A = 41A$$

Since the maximum output from the PV cells seldom occurs simultaneously as the maximum output from the wind turbines, the maximum current is chosen to $30A$ for the bi-directional converter. For this converter, both the current ripple, Δi_L, and the boundary current, I_{oB} is set to $0.1A$.

In the bidirectional converter there are two capacitors, C_H and C_L, as can be seen in figure 2.10. C_H is designed for the boost converter, when the battery discharge, and C_L is designed for the buck converter, when the battery is charging. Since there is only one inductor, its values are calculated for both cases and selected as the highest value.

5.4 Snubber Design

Parasitic elements, in shape of stray inductances, are added to the converter circuits to resemble a more realistic scenario. For the buck and the boost converter, the inductance connected to the diode is assumed to be $10nH$ and $15nH$ for the inductance connected to the switch. As for the bi-directional converter, both the stray inductances are assumed to be $15nH$. These values are estimations based upon the length of the copper wire between different components and would be different if the circuit is realized, however, the ones selected here fulfill a demonstrating purpose.

For each converter, two snubbers are designed. For the buck and the boost converter, a turn-off snubber and a diode snubber are designed, but those snubbers are complicated to implement for the bidirectional converter. Since the diodes and the switches in the bidirectional converter are connected in parallel to each other, they would affect a snubber placed in parallel. Therefore are turn-on snubbers selected and designed for this converter instead of turn-off snubbers or diode snubber. This is because turn-on snubbers are connected in series to the semiconductors instead of in parallel.

All snubbers are designed according to the equations presented in section 2.7.1 and 2.7.2. In `LTSpice`, voltage and current waveforms are analyzed at the rated power of $260W$. The unknown variables that are needed for the equations are extracted through observations.

6

Systems for the Different Modes and Locations

In this chapter, results that are related to the system sizing is presented. Possible wind- and solar power generation combinations are presented to understand different scenarios. The battery size is also included and will be presented for each individual system. For each location, two results will be presented, one for the continuous case and one for the interval operation. To analyze the energy harvesting possibilities, the data which is presented in figure 4.1, 4.2 and 4.3 is used.

6.1 System Model

The models designed in chapter 4 are combined into a full system model, as can be seen in figure 6.1. The produced power is compared with the required power of the radar, and if the power produced is higher than the load power, the battery is charged, otherwise the battery is discharged. In figure 6.1, the block with the notation "PE" represent power electronic converters and is set to the efficiency with its associated snubber design. The efficiencies of the converters are presented in section 7.2, table 7.3.

With wind speed and solar radiation as input, the state of charge in the battery can be analyzed. By analyzing different wind- and solar power combinations, an estimation of the battery size can be carried out for each case. What is not seen in figure 6.1 is that the PV and the battery model take the temperature into consideration.

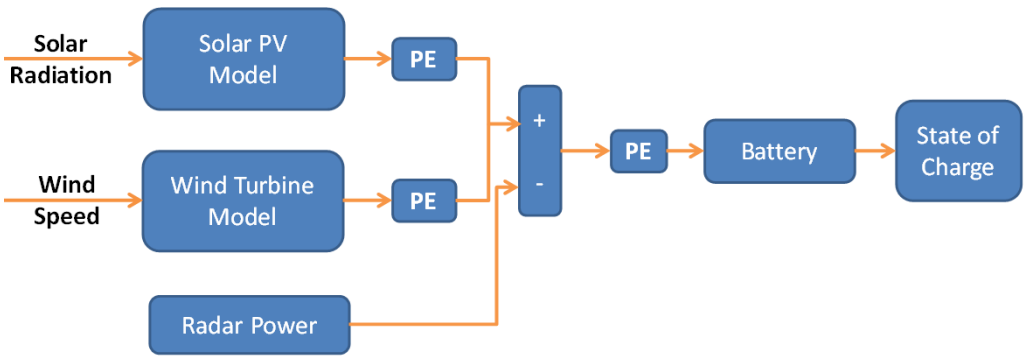

Figure 6.1: Simplified model of the system.

In section 4.2, 4.3 and 4.4, the cost and area requirements for each individual component is presented. The cost of the system is divided into different parts and with the use of table 6.1, an overview of the cost for each part of the system can be noticed. Essentially, the ESS is an expensive part of the system, as a large battery is needed to compensate for the intermittent characteristics in renewable energy production.

Table 6.1: Cost and area of the individual parts of the system.

	PV cell	HAWT	VAWT	Battery
$	$210/product$	$300/product$	$250/product$	$90/kWh$
Area $[m^2]$	1.67	3	1	-

6.2 The System in Gothenburg

In Gothenburg, neither of the chosen power generating technologies are able to provide enough energy by themselves without a large battery. Generation parameters are set for each presented system and the battery is changed to find the least energy capacity needed to make the system feasible.

6.2.1 Continuous Operation

This section present a set of possible solutions which could be used in Gothenburg under continuous radar operation, presented in chapter 3. In table 6.2, the result is shown and columns related to the power generation is represented in quantity of the selected product and its individual cost. The last three columns present: the battery energy capacity adn its associated cost, the total area required for the power generation and lastly, the cost which make the system possible.

Table 6.2: Possible energy harvesting systems in Gothenburg if the radar require continuous operation.

Solar Cells ($)	Vertical Turbines ($)	Horizontal Turbines ($)	Battery [kWh]	Area $[m^2]$	Total Cost $[\$K]$
0 ($0)	0 ($0)	1 ($300)	714 (64.2K$)	3	64.5
0 ($0)	1 ($250)	1 ($300)	277 (24.9K$)	4	25.5
0 ($0)	0 ($0)	2 ($600)	165 (14.8K$)	6	15.4
3x1 ($630)	0 ($0)	1 ($300)	178 (16.0K$)	8	16.9
3x2 ($1260)	1 ($250)	1 ($300)	89 (8.0K$)	14	9.8
3x2 ($1260)	0 ($0)	2 ($600)	51 (4.6K$)	16	6.5
3x3 ($1890)	0 ($0)	0 ($0)	∞	15	∞
3x8 ($5040)	0 ($0)	0 ($0)	647 (58.2K$)	40	63.2

From table 6.2 it can be seen that a combination of wind- and solar power generation yields the smallest battery capacity needed. With only wind power, the required

battery energy capacity is still large but significantly smaller compared to the case when only a PV system is used. The energy capacity needed if only wind power is used, is comparable to more than two electric bus batteries, which was presented in section 2.5.1.

From observations regarding the power production of each individual technology, it can been noted that a large amount of solar power is produced during the summer, but a minimal amount is produced during the winter. This is the reason why such a large battery is required for a PV system. It is also important to notice that a PV system with a $3x3$ configuration do not meet the total power demand and the battery need to be infinity large due to this. Additionally, in figure 6.2a, the power production from a $3x4$ PV module is presented and how the solar irradiation vary with seasons can clearly be noted.

With only wind power generation, it can be seen from table 6.2 that it requires a large battery pack to be feasible. A system which only utilize wind power production is presented in figure 6.2b and compared to a PV system it can be observed that the power production from the wind system only follow some seasonal variations, as it have a more concentrated wind speeds during the winter. The best presented wind system use two horizontal wind turbine.

By combining the models, the power production can be seen in figure 6.2c. The best combined system in terms of energy capacity and cost is presented in table 6.2 and use a $3x2$ PV module and two horizontal wind turbines. Important to notice is that the periods when the system produce less than the required $260W$ are few and short, which result in a smaller battery. The required energy capacity for the battery is $51kWh$ and compared to other presented result, it has significantly been reduced. As the battery is the system's most expensive component, it is necessary to minimize the size of the battery so the system is economically feasible. Additionally, a rough estimation of the area needed for the system is presented in table 6.2 and it can be seen that for a combination system, the area is also reduced compared to when only using a PV system. A combined system is thus the most adequate and appropriate choice of system configuration to use in this case.

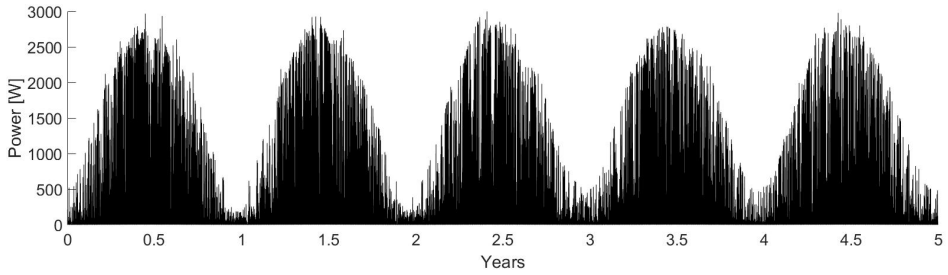

(a) Solar power generation during several years in Gothenburg.

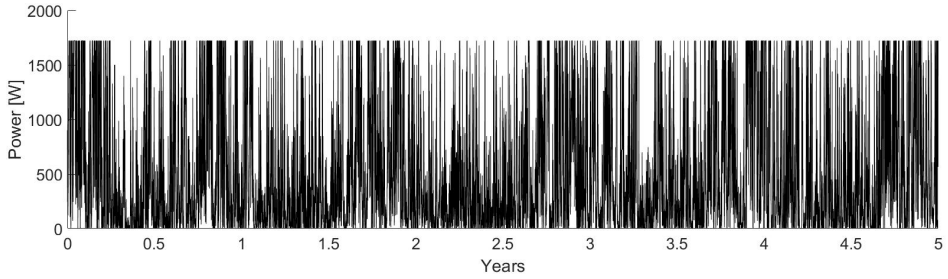

(b) Power production from two vertical- and one horizontal- wind turbine(s).

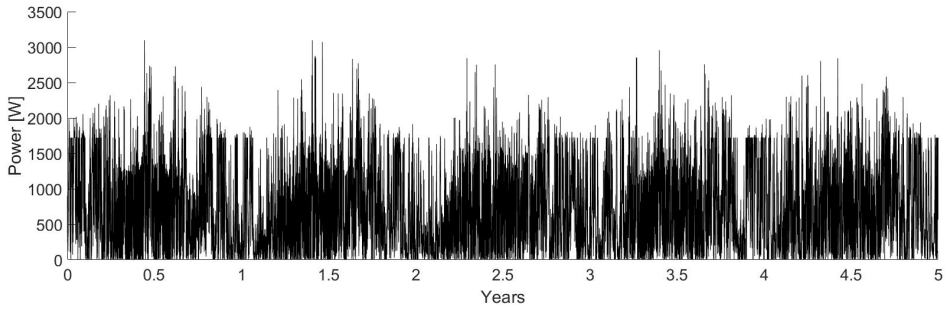

(c) How the power production of a combined system may look like.

Figure 6.2: Power production in Gothenburg under continuous operation.

A combined system resulted in the lowest battery energy capacity and the capacity is determined so the battery is never depleted. In figure 6.3, the combined system battery's SOC is displayed and it is possible to see a few interesting periods. After around one year, during a winter, the system is not able to meet the power demand. The battery starts to discharge and therefore the SOC starts to drop. The same behavior can be seen at each winter season and this is due to the solar power production, as it produce an almost negligible amount of power during certain periods of the winter. There are day-to-day changes and they can be noticed from the ripple around 90% SOC. At these times, the battery is charged and discharged back and forth.

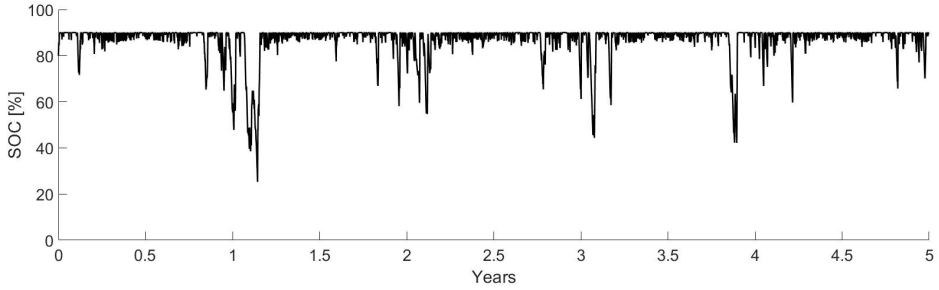

Figure 6.3: Display how the SOC of the battery change with time.

6.2.2 Interval Operation

When using an interval operation, the average power demand is lower and the system is smaller. From table 6.3 it can be observed that a combined system yield the smallest battery, which was the same observation as in section 6.2, but compared to the continuous case it have been scaled down as a result of the reduced power demand.

Table 6.3: Possible energy harvesting systems in Gothenburg for interval operation.

Solar Cells	Vertical Turbines	Horizontal Turbines	Battery [kWh]	Area $[m^2]$	Total Cost [$\$K$]
0 ($0)	1 ($250)	0 ($0)	116 (10.4K$)	1	10.7
0 ($0)	0 ($0)	1 ($300)	27 (2.4K$)	3	2.7
0 ($0)	1 ($250)	1 ($300)	22 (2.0K$)	4	2.6
0 ($0)	0 ($0)	2 ($600)	20 (1.8K$)	6	2.4
3x1 ($630)	0 ($0)	0 ($0)	357 (32.1K$)	5	32.8
3x1 ($630)	1 ($250)	0 ($0)	25(2.2K$)	6	3.1
3x1 ($630)	0 ($0)	1 ($300)	8 (0.7K$)	8	1.6
3x2 ($1260)	0 ($0)	0 ($0)	245 (22.0K$)	10	23.3
3x3 ($1890)	0 ($0)	0 ($0)	178 (16.0K$)	15	17.9

For interval operation, using only a PV system is considerably more feasible than for the continuous case. The required battery energy capacity can be reduced to $178kWh$ with a $3x3$ solar cell configuration. Due to economical factors, large batteries are not desirable as they are a large investment. Instead, if a system only utilize a HAWT, it is able to provide the power with a small battery of $27kWh$. From table 6.3 it can be seen that by using two HAWTs compared to using one HAWT, the energy capacity can be reduce by $7kWh$, which is a small reduction compared to the additional energy provided. Hence, if only a wind power system is of interest, a HAWT would be the best choice.

When an interval based operation is used, the required energy capacity, the needed area and cost have been reduced. Table 6.3 presents a combined system which use

one HAWT and $3x1$ PV cells. This system have a small battery and low cost, and as was shown for the continuous case, the combined system has an advantage over using only one source of power. Therefore, a combined system is desired in this application too, as it helps to minimize the cost and keep the land occupation small.

6.3 Sde Boker

Sde Boker's climate is different compared to Gothenburg and because of that, other system configurations will be of interest. From figure 4.3, the wind speed for Sde Boker can be seen and it does not reach any high velocities. The irradiation can be seen in figure 4.2 and Sde Boker has a much higher value than Gothenburg. During the winter season, the irradiation in Sde Boker is almost comparable to the irradiation in Gothenburg during the summer season. Solar PV generation will therefore be the superior source of power generation in Sde Boker.

6.3.1 Continuous Operation

When the radar operates under continuous conditions and require $260W$, it yields the result which is presented in table 6.4. The presented result include the generation technology, the necessary battery energy capacity and finally the corresponding area and cost. The principle behind table 6.4 is the same as mentioned in section 6.2, and will be used to analyze the possibilities for the system.

Table 6.4: Possible energy harvesting systems in Sde Boker if the radar require continuous operation.

Solar Cells	Vertical Turbines	Horizontal Turbines	Battery [kWh]	Area $[m^2]$	Total Cost [$\$K$]
0 ($0)	0 ($0)	5 ($1500)	∞	15	∞
3x1 ($630)	0 ($0)	0 ($0)	∞	5	∞
3x2 ($1260)	0 ($0)	0 ($0)	156 (14.0K$)	10	15.3
3x2 ($1260)	0 ($0)	1 ($300)	62 (5.6K$)	13	7.2
3x2 ($1260)	1 ($250)	1 ($300)	49 (4.4K$)	14	6.2
3x3 ($1890)	0 ($0)	0 ($0)	40 (3.6K$)	15	5.5
3x3 ($1890)	1 ($250)	0 ($0)	18 (1.6K$)	16	3.8
3x5 ($3150)	0 ($0)	0 ($0)	28 (2.5K$)	25	5.7

The solar PV generations dominance can clearly be seen from table 6.4 and it can be noted that PV cells are an essential component for a harvesting system located in Sde Boker or a similar environment. A wind turbine system alone is not to be prefered. From figure 4.3, the wind speed data of Sde Boker is presented. As the average value and the standard deviation of the wind speed is low, the wind turbines seldom operates where it can contribute with a significant power.

The high energy harvesting potential in Sde Boker is mainly due to its high amount of solar irradiation. Figure 6.4 display the power production for a $3x3$ PV system and from the figure it is possible to see that the solar power produced in Sde Boker follow the same seasonal relationship that was mentioned for Gothenburg, but it has higher values. This directly correlates to the result presented in table 6.4 and can with the help of figure 6.4, show that a PV system is able to achieve a dense power production over the entire simulated period. With an addition of wind turbines, the power production curve will be even denser and therefore, a smaller battery can be used. For Sde Boker, it can be seen that only a PV based system could be implemented, but by adding a wind turbine, the cost is reduced.

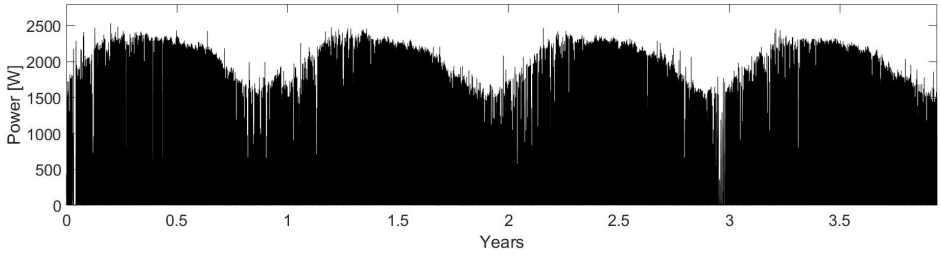

Figure 6.4: Display the power production of a $3x3$ PV system in Sde Boker.

6.3.2 Interval Operation

The same principle apply for the interval case as for the continuous case. From table 6.5 it can be seen that the energy capacities for the batteries are small for all the presented configurations but for a combination system, the battery energy capacity is reduced the most. It reached as low as to have a energy capacity of $4kWh$ and with a total system cost of \$1240. It is also possible to notice that there is a small difference between the three configurations, the best choice should depend on the available area and the budget. The three best systems are the ones with $3x1$ PV cells. The first one is without a wind turbine, the second with a vertical turbine and the third with a horizontal turbine. The systems with combined wind- and solar power production have a lower cost but the one with only PV-cells is simpler as it only requires one source of power.

Table 6.5: Possible energy harvesting systems in Sde Boker if the radar operate with intervals.

Solar Cells	Vertical Turbines	Horizontal Turbines	Battery [kWh]	Area $[m^2]$	Total Cost [\$$K$]
2x1 (\$420)	0 (\$0)	0 (\$0)	49 (\$4.4K)	3	4.8
3x1 (\$630)	0 (\$0)	0 (\$0)	14 (\$1.3K)	5	1.9
3x1 (\$630)	1 (\$250)	0 (\$0)	4 (\$0.36K)	6	1.2
3x1 (\$630)	0 (\$0)	1 (\$300)	4 (\$0.36K)	8	1.3
3x2 (\$1260)	0 (\$0)	0 (\$0)	9 (\$0.81K)	10	2.1

6.4 Thule

The climate of Thule sets a high demand on the energy harvesting system. The irradiation is similar to Gothenburg during the summer but during the winter, the irradiation is very low for a long period of time, can be seen in figure 4.2. The wind speeds are in between the levels of Sde Boker and Gothenburg and are neither great nor bad. With a long night during the winter, solar power is expected to be inferior, but it is still investigated. In this section, the validity of the model is questioned due to the climate. The result presented here might be an underestimation because additional thermal management system is not taken into consideration.

6.4.1 Continuous Operation

In continuous operation, the system in Thule needs to be significantly larger than for Gothenburg and Sde Boker. This is because it is difficult to produce enough power and to keep a high power density over the years. In table 6.6, the results from Thule is presented. Wind power is noticeably favoured over solar power as the system with only PV cells requires a larger battery. According to table 6.6, a system with $3x6$ solar cells and four HAWTs are to be preferred. This system requires a battery of $357kWh$ and the total cost of \$36900.

Table 6.6: Possible energy harvesting systems in Thule if the radar require continuous operation.

Solar Cells	Vertical Turbines	Horizontal Turbines	Battery [kWh]	Area $[m^2]$	Total Cost [\$$K$]
0 (\$0)	0 (\$0)	3 (\$900)	∞	9	∞
0 (\$0)	0 (\$0)	4 (\$1200)	536 (\$48.2K)	12	49.4
0 (\$0)	0 (\$0)	5 (\$1500)	446 (\$40.1K)	15	41.6
3x6 (\$3780)	0 (\$0)	0 (\$0)	1562 (\$140.6K)	30	144.4
3x6 (\$3780)	0 (\$0)	2 (\$600)	580 (\$52.2K)	36	56.6
3x6 (\$3780)	0 (\$0)	4 (\$1200)	357 (\$32.1K)	42	37.1
3x100 (\$63K)	0 (\$0)	0 (\$0)	1071 (\$96.4K)	503	159.4
3x100 (\$63K)	0 (\$0)	5 (\$1500)	245 (\$22.0K)	518	86.5

Overall, a system in Thule which is designed for continuous operation is not realistic. The impact of the increased system size and price is the reason why the system is unrealistic. The application area in Thule is probably not that hectic and a continuous operation is unlikely necessary to be used here.

6.4.2 Interval Operation

Transitioning to the interval operation, the size of the proposed systems have a reasonable size compared to the continuous operation case and is comparable to the systems for the other locations. The result is shown in table 6.7 and a system with only solar power is discarded immediately as the price for the configuration is far

more expensive. When using two of both VAWTs and HAWTs, it did not help to extend the system with more solar cells, which showcases the favoritism of wind turbines in this climate. This can be explained by the fact that the wind speed has a period with low velocities during the winter, when the PV cells do not contribute. A system which use two of both VAWTs and HAWTs would be desirable for this scenario.

Table 6.7: Possible energy harvesting systems in Thule if the radar operate with intervals

Solar Cells	Vertical Turbines	Horizontal Turbines	Battery [kWh]	Area [m^2]	Total Cost [$\$K$]
0 ($0)	0 ($0)	1 ($300)	178 (16.0K$)	3	16.3
0 ($0)	2 ($500)	2 ($600)	52 (4.7K$)	8	5.8
3x1 ($630)	0 ($0)	0 ($0)	580 (52.2K$)	5	52.8
3x1 ($630)	0 ($0)	1 ($300)	152 (13.7K$)	8	14.6
3x2 ($1260)	0 ($0)	0 ($0)	491 (44.2K$)	10	45.5
3x2 ($1260)	2 ($500)	2 ($600)	52 (4.7K$)	18	7.1
3x3 ($1890)	0 ($0)	0 ($0)	446 (40.1K$)	15	42.0

6.4.3 Climate Concerns

Temperatures in Thule are extremely low in comparison to Gothenburg and Sde Boker and during the winter, it can reach below -30°C. All parts of the system need to be able to handle these temperature, else thermal management systems are needed. According to the guidelines in section 4.3, an ice prevention system is required for Thule.

The model uses a battery and in these temperatures, batteries struggle to operate and would also need a thermal management system. Heating up a large battery would be necessary for Thule and would be an additional cost, increase the power demand and increase the area needed. In this case, it could be of value to investigate further into other ESS technologies, like hydrogen storage. The poor efficiency of a hydrogen storage results in plenty of thermal losses which potentially could be used to heat up other parts of the system.

6.5 Environmental Analysis

Current off-grid energy systems for radars use fossil fuel combustion engines due to the availability, simplicity and reliability but do not consider the environmental impact. The use of renewable energy sources instead of fossil fuel is an improvement in the sustainable aspect and help to reduce the emissions. As renewable energy sources emit no emissions during its operation, the material which is used in the system is of greater importance to help reduce the environmental footprint.

For this renewable system, a LFP battery was selected as it is one of the LiB types with the smallest environmental impact. Since the battery is both an expensive part of the system and that the material supply is limited, it is recommended to have a small battery, but within reasonable power production sizes. The PV cells is another part of the system which have an environmental impact during its manufacturing. It is therefore recommended to use highly efficient PV cells, so the required material is lesser.

7
Converters and snubbers

The components for each converter are presented in the following section with their associated efficiencies. To give a coherent understanding of the snubbers effect on the designed converters, the voltage and the current waveforms for the boost converter's semiconductors will be presented. One scenario is without the snubbers and one is with snubbers to pinpoint the differences. Additionally, how the designed snubbers effect the efficiency of the converters will be presented and discussed to understand the impact of using snubbers in the presented system.

7.1 Converters

The buck-, the boost- and the bidirectional converterter are designed as described in chapter 5, and the component values are presented in table 7.1. With regards to the parasitic elements, values of real components are selected and added into the simulation model in `LTSpice`. The selected components bring non-ideal elements such as ESR, which is unique for each component. In table 7.1, the parameters L_{esr} and C_{esr} are presented and represent the ESR for respective component. The ESR value is taken from already existing components which could be used in the converters.

Table 7.1: Display the calculated and selected values for the components.

		L [μH]	C_H [μF]	C_L [nF]	L_{esr} [mΩ]	C_{esr} [mΩ]
Buck	Calculated	140	-	139	-	-
Converter	Selected	400	-	300	3.8	2
Boost	Calculated	15.8	8.64	-	-	-
Converter	Selected	40	10	-	3.8	2
Bidirectional	Calculated	107	12.9	52.1	-	-
Converter	Selected	400	15	100	3.8	1

7.2 Effect of Snubbers

In table 7.2, the calculated and chosen component values which are related to the snubbers are presented. Comparing these values, the chosen value is generally larger than the calculated. As the calculations are based upon values from observations, there is a potential error in the calculations. By trial and error, the snubber design is changed to achieve better result. In table 7.2, there are two elements which are presented with a '−', and this is because the value is calculated with parameters which need to be found in the current waveform. They are therefore considered as design choices and not calculated values.

Table 7.2: Display the calculated and chosen values for the different snubbers.

		R_{di} [Ω]	C_{di} [pF]	R_{sw} [Ω]	C_{sw} [nF]
Buck Converter	Calculated	16.8	59.7	27.68	2.70
	Selected	17.1	58	30	2.70
Boost Converter	Calculated	12.14	115	20.77	0.356
	Selected	12.38	110	29.3	0.744
		R_{sw1} [Ω]	L_{sw1} [nH]	R_{sw2} [Ω]	L_{sw2} [nH]
Bidirectional Converter	Calculated	-	160	-	15
	Selected	7	160	5	15

The values presented in table 7.2 relate back to figure 2.12 and figure 2.13. For the bidirectional converter, turn-on snubbers are used instead of turn-off snubbers. Resistance, R_{sw1}, and inductance, L_{sw1}, which is presented in table 7.2, are used in the snubber which is related to switch $S1$, see figure 2.10. The remaining resistance, R_{sw2}, and inductance, L_{sw2}, are instead related to switch $S2$.

For the boost converter, the snubber reduced the oscillations at both the diode and the switch, which can be seen in figure 7.1. It also suppressed the voltage overshoot over the switch. An additional point which can be noticed from figure 7.1 is that the rise time for both the current and voltage at the switch have been increased because of the use of a turn-off snubber. The peak value have decreased and reduced the overall rate of which the voltage and the current rise. By reducing the oscillations and suppressing the overshoot of the voltage and the current, the stress which the semiconductor is subjected to, is reduced. Snubbers which are connected to semiconductors, help to decrease the stress and to increase the lifetime of the semiconductor.

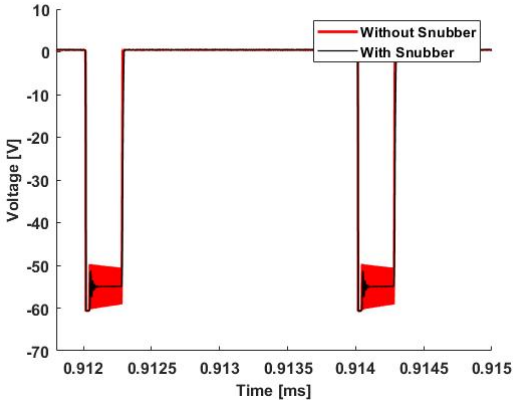

(a) Voltage over a diode with and without an snubber.

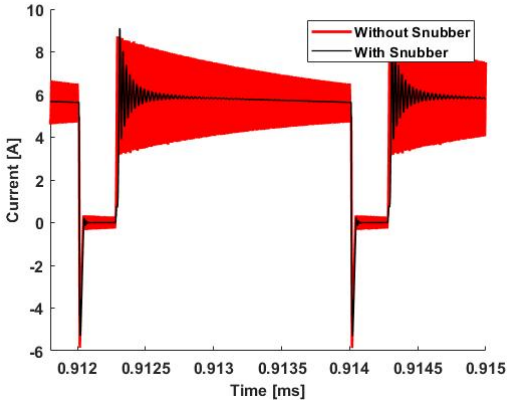

(b) Current through a diode with and without an snubber.

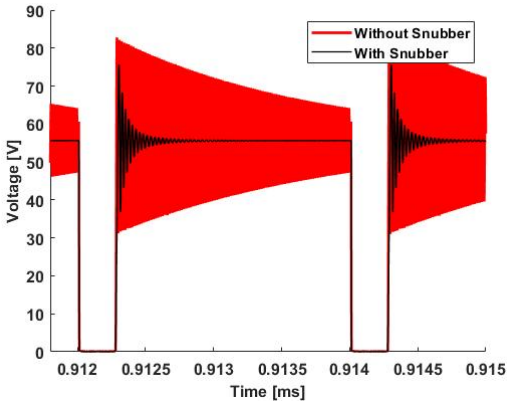

(c) Voltage over a switch with and without an snubber.

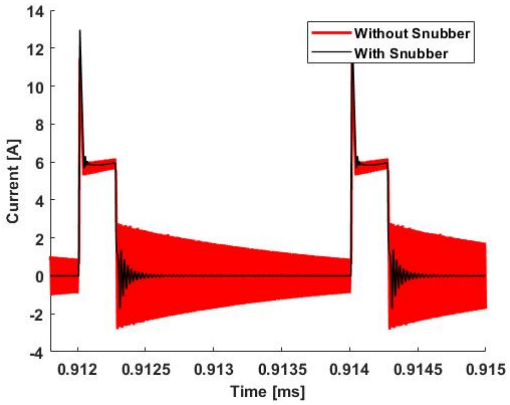

(d) Current through a switch with and without an snubber.

Figure 7.1: The snubber's effect on the waveforms at the diode in the boost converter.

For each converter, the designed snubbers achieve similar effect and help to reduce the stress for the semiconductors. The majority of the converters lose efficiency at rated power[12] due to the snubbers, which can be seen in table 7.3. For the bidirectional converter, when it operates in buck mode, its efficiency is increased by 8% and reach 97.2% in the simulations. The reason why the efficiency increases is due to the two turn-on snubbers. They help to reduce the the majority of the losses during the switching event. For the designed bidirectional converter when operating in buck mode, the majority of its losses occurred during the turn-on event and because those losses have been reduced, the efficiency increased significantly due to this.

When designing snubbers, the focus have been to reduce the stress which affect the semiconductors and to minimize the losses related to them. It is hence necessary to balance or weight what is the most important. It is not always necessary to use snubbers, and depending on the chosen semiconductor and the specifics of the

[12]When the power at the receiving load is $260W$.

circuit, it may not be required. If the chosen semiconductor is able to handle the stress which it is subjected to, additional components can result in a significant efficiency loss and only a small reduction in terms of stress. It is thus important to chose semiconductors with care, and to analyze the circuit before deciding to design snubbers.

Table 7.3: The efficiency for the converters, with and without snubbers connected.

	Without Snubber [%]	With Snubber [%]
Boost Converter	98.3	97.9
Buck Converter	91.2	91
Bidirectional Buck Mode	89.1	97.2
Bidirectional Boost Mode	96.8	94.5

8

Recommendations and Future Work

The report have worked toward giving a recommendation to SAAB regarding the potential of using an off-grid energy harvesting system to operate radar equipment. From chapter 6 it was presented that all investigated locations can be used, but with different result.

This chapter presents the conclusion of the report and give system recommendations for each of the investigated locations. Power electronics will also be addressed and a recommendation will be given. Lastly, a section regarding the future and what parts of the system which would need additional investigations are presented.

8.1 Conclusion

For the system in Gothenburg, it is recommended to use a hybrid system which use both solar energy and wind energy. The recommended system configuration for the continuous case and the interval is displayed in table 8.1. The recommended systems have low system costs, and from the costs it could be concluded that the battery was the most expensive component in the system. Additionally, by using a hybrid system, it was concluded that the two harvesting technologies could compensate each other's shortcomings over the seasons.

In Sde boker, the potential of using solar power was the highest. A solar system would be able to achieve a continuous operation in the case that enough area is available and founds are sufficient. Wind power was not preferred to use on its own, but could help to reduce the system cost. It is therefore recommended to use a hybrid system in Sde Boker too, which can be seen in table 8.1.

Regarding the system in Thule, continuous operation cycle for the radar is not recommended. The cost and size of such a system would be enormous. Instead, an interval operation cycle is more appropriate to use in Thule. From the result it was noted that a wind turbine system was essential to minimize the cost and area required. Unfortunately, the climate in Thule require the wind turbines to have an ice preventing system and thermal management systems, which result in an additional required power. This extra power demand is not taken into account and will cause the result to not reflect the reality. It is therefore recommended to

do a more in-depth analysis regarding the ice preventing system before expressing a recommended system configuration.

Table 8.1: The recommended systems for each location and operation mode.

	Continuous Case			Interval Case		
	PV	VAWT	HAWT	PV	VAWT	HAWT
Gothenburg	3x2	0	2	3x1	0	1
Sde Boker	3x3	1	0	3x1	1	0
Thule	-	-	-	0	2	2

The power electronics in the system are all done in a simulation environment and from the result and investigation, it have been proven that the need for efficient converters are important. From the result presented in chapter 7, a highly efficient converter could be simulated in `LTSpice`, but the reality may not be the same. It is therefore recommended to build prototypes and perform tests before knowing if the designed converter meet the requirements and the expectations. As for the snubbers, they can only properly be designed on real converters were parasitic elements are present.

8.2 Future Work

From the generated model, evaluations regarding what kind of system that could be the best was made. Important to take into account is that assumptions have been made and how they may effect the result of the report. To achieve a more accurate result which reflects reality, it will be necessary to redo the models without the assumptions.

All the results for the off-grid harvesting system are based upon the available weather data, but as the reality is always changing, it may not be necessary to assume that the designed system is able to overcome the future. This will always be a problem but can be limited by field testing. For this, a prototype of the system is needed and unfortunately this was not included in the project. It is recommended to create a prototype before finalizing if it is possible to have an off-grid harvesting system at a given location. The model is created as a guideline, but with a prototype and testing, it would be possible to generate a more accurate conclusion.

For the wind- and the solar model, ancillary components have been looked into but not analyzed nor implemented into the models. Instead, it was assumed that the MPPT and the yaw control follow the pre-set design choices. In a realistic environment, the ancillary components and the control schematics are not able to fully follow the behavior which is presented in a simulation. Additional investigations and simulations thus need to be done to implement the MPPT and the yaw control into the solar model and wind model respectively.

Finally, the control over the power electronics and the system need to be investigated in-depth. The generated system assumes that the control loops are working and help to adjust each converters duty cycle to stabilize the voltage over the radar in the case of a disturbance. To generate a complete system, it is necessary to look into possible solutions of how to best control the system. An interesting possibility would be to investigate the use of $A.I$, and use it as the highest decision making entity in the system.

Bibliography

[1] S. Guo, H. Zhao, and H. Zhao, "The most economical mode of power supply for remote and less developed areas in China: Power grid extension or microgrid?", *Sustainability (Switzerland)*, vol. 9, no. 6, 2017, ISSN: 20711050. DOI: 10.3390/su9060910.

[2] A. Hirsch, Y. Parag, and J. Guerrero, "Microgrids: A review of technologies, key drivers, and outstanding issues", *Renewable and Sustainable Energy Reviews*, vol. 90, no. April, pp. 402–411, 2018, ISSN: 18790690. DOI: 10.1016/j.rser.2018.03.040. [Online]. Available: https://doi.org/10.1016/j.rser.2018.03.040.

[3] J. Ehnberg, H. Ahlborg, and E. Hartvigsson, "Flexible distribution design in microgrids for dynamic power demand in low-income communities", *IEEE PES PowerAfrica Conference, PowerAfrica 2016*, pp. 179–183, 2016. DOI: 10.1109/PowerAfrica.2016.7556596.

[4] E. Hartvigsson, E. Ahlgren, and J. Ehnberg, "Rural Electrification Through Minigrids in Developing Countries : Initial Generation Capacity Effect on Cost- - Recovery", *Publish Reaserch Chalmers*, pp. 1–12, 2013.

[5] S. Bhattacharyya, *Rural Electrification Through Decentralised Off-grid Systems in Systems in Developing Countries*, 4th ed., S. Bhattacharyya, Ed. Leicester: Springer, 2012, pp. 13–186, ISBN: 9781608052851. DOI: 10.2174/97816080528511120101. [Online]. Available: http://www.eurekaselect.com/102081/volume/1.

[6] C. Nayar, "Innovative Remote Micro-Grid Systems", *International Journal of Environment and Sustainability*, vol. 1, no. 3, pp. 53–55, 2012.

[7] S. C. Bhattacharyya, "Energy access programmes and sustainable development: A critical review and analysis", *Energy for Sustainable Development*, vol. 16, no. 3, pp. 260–271, 2012, ISSN: 09730826. DOI: 10.1016/j.esd.2012.05.002. [Online]. Available: http://dx.doi.org/10.1016/j.esd.2012.05.002.

[8] S. Ashok, "Optimised model for community-based hybrid energy system", *Renewable Energy*, vol. 32, no. 7, pp. 1155–1164, 2007, ISSN: 09601481. DOI: 10.1016/j.renene.2006.04.008.

[9] S. Ur Rehman, S. Rehman, M. U. Qazi, M. Shoaib, and A. Lashin, "Feasibility study of hybrid energy system for off-grid rural electrification in southern Pakistan", *Energy Exploration and Exploitation*, vol. 34, no. 3, pp. 468–482, 2016, ISSN: 20484054. DOI: 10.1177/0144598716630176.

[10] B. Bhandari, K. T. Lee, C. S. Lee, C. K. Song, R. K. Maskey, and S. H. Ahn, "A novel off-grid hybrid power system comprised of solar photovoltaic, wind,

and hydro energy sources", *Applied Energy*, vol. 133, no. November, pp. 236–242, 2014, ISSN: 03062619. DOI: 10.1016/j.apenergy.2014.07.033. [Online]. Available: http://dx.doi.org/10.1016/j.apenergy.2014.07.033.

[11] C. Brandoni and M. Renzi, "Optimal sizing of hybrid solar micro-CHP systems for the household sector", *Applied Thermal Engineering*, vol. 75, pp. 896–907, 2015, ISSN: 13594311. DOI: 10.1016/j.applthermaleng.2014.10.023.

[12] B. C. Donovan, D. J. McLaughlin, M. Zink, and J. Kurose, "OTGsim: Simulation of an off-the-grid radar network with high sensing energy cost", *2008 5th Annual IEEE Communications Society Conference on Sensor, Mesh and Ad Hoc Communications and Networks, SECON*, pp. 509–514, 2008. DOI: 10.1109/SAHCN.2008.67.

[13] D. Richardson, "AESA Radar Technology", *Armada International*, vol. 3, 2015.

[14] SAAB, "Giraffe 8A Aesa 3D Long Range Radar", Sweden, [Online]. Available: https://saab.com/globalassets/commercial/air/sensor-systems/ground-based-air-defence/giraffe-8a/giraffe_8a_product_folder.pdf%20D:0:A:%202019-05-23.

[15] J. Abraham and B. Plourde, *Small-Scale Wind Power : Design, Analysis, and Environmental Impacts*, 3rd ed. Minnesota: Momentum Press, 2014, pp. 1–20.

[16] J. Sarshar, S. S. Moosapour, and M. Joorabian, "Multi-objective energy management of a micro-grid considering uncertainty in wind power forecasting", *Energy*, vol. 139, pp. 680–693, 2017, ISSN: 03605442. DOI: 10.1016/j.energy.2017.07.138. [Online]. Available: https://doi.org/10.1016/j.energy.2017.07.138.

[17] H. L. Zhang, J. Baeyens, J. Degrève, and G. Cacères, "Concentrated solar power plants: Review and design methodology", *Renewable and Sustainable Energy Reviews*, vol. 22, pp. 466–481, 2013, ISSN: 13640321. DOI: 10.1016/j.rser.2013.01.032.

[18] M. Liu, N. H. Steven Tay, S. Bell, M. Belusko, R. Jacob, G. Will, W. Saman, and F. Bruno, *Review on concentrating solar power plants and new developments in high temperature thermal energy storage technologies*, 2016. DOI: 10.1016/j.rser.2015.09.026.

[19] D. Barlev, R. Vidu, and P. Stroeve, "Innovation in concentrated solar power", *Solar Energy Materials and Solar Cells*, vol. 95, no. 10, pp. 2703–2725, 2011, ISSN: 09270248. DOI: 10.1016/j.solmat.2011.05.020. [Online]. Available: http://dx.doi.org/10.1016/j.solmat.2011.05.020.

[20] Alexchris, *Type of Concentrated Solar Power*, 2011. [Online]. Available: https://commons.wikimedia.org/wiki/File:Type_of_Concentrated_solar_power.png.

[21] M. A. Green, K. Emery, D. L. King, S. Igari, and W. Warta, "Solar cell efficiency tables (version 52)", *Progress in Photovoltaics: Research and Applications*, 2018. DOI: 10.1002/pip.574.

[22] B. Parida, S. Iniyan, and R. Goic, *A review of solar photovoltaic technologies*, 2011. DOI: 10.1016/j.rser.2010.11.032.

[23] P. Hersch, K. Zweibel, and S. Energy Research Institute, "Basic Photovoltaic Principles and Methods", U.S Department of Energy, Colorado, Tech. Rep., 1982, pp. 1–71. DOI: SERI/SP-290-1448.

[24] M. G. Villalva, J. R. Gazoli, and E. Ruppert Filho, "Modeling and circuit-based simulation of photovoltaic arrays", in *2009 Brazilian Power Electronics Conference, COBEP2009*, 2009, ISBN: 9781424433704. DOI: 10.1109/COBEP.2009.5347680.

[25] I. V. Banu, R. Beniugă, and M. Istrate, "Comparative Analysis of the Perturb-and-Observe and Incremental Conductance MPPT Methods", *The 8th International Symposium On Advanced Topics In Electrical Engineering Comparative*, pp. 1–4, 2013.

[26] J. P. Abraham and B. Plourde, "Small-Scale Wind Power : Design, Analysis, and Environmental Impacts", in *Small-Scale Wind Power : Design, Analysis, and Environmental Impacts*, New York: Momentum Press, 2014, ch. 1-2, pp. 1–44, ISBN: 978-1-60650485-7. DOI: 10.5643/9781606504857.

[27] Scott Davis, *Wattle Point wind farm near Edithburgh*, 2005. [Online]. Available: https://commons.wikimedia.org/wiki/Wind_turbine#/media/File:Wattle_Point_windmill.jpg.

[28] Dingley Andy, *Vertical-axis wind turbine, installed at Rogiet primary school*, 2010. [Online]. Available: https://commons.wikimedia.org/wiki/File:Quietrevolution_qr5,_Rogiet_school.jpg.

[29] K. Pope, I. Dincer, and G. F. Naterer, "Energy and exergy efficiency comparison of horizontal and vertical axis wind turbines", *Renewable Energy*, 2010, ISSN: 09601481. DOI: 10.1016/j.renene.2010.02.013.

[30] E. Dick, "Wind turbines", *Fluid Mechanics and its Applications*, 2015. DOI: 10.1007/978-94-017-9627-9{_}10.

[31] L. Battisti, *Wind Turbines in Cold Climates Icing Impacts and Mitigation Systems*. Springer International Publishing, 2015, pp. 1–4, ISBN: 978-3-319-05191-8. DOI: 10.1007/978-3-319-05191-8. [Online]. Available: http://www.springer.com/series/8059.

[32] H. Ramenah and C. Tanougast, "Reliably model of microwind power energy output under real conditions in France suburban area", *Renewable Energy*, 2016, ISSN: 09601481. DOI: 10.1016/j.renene.2015.11.019.

[33] F. Farret, L. Pfischer, and D. Bernardon, "Active yaw control with sensorless wind speed and direction measurements for horizontal axis wind turbines", 2002. DOI: 10.1109/iccdcs.2000.869856.

[34] A. Y. Joshi and S. G. Soni, "Design of Active Yaw Control Mechanism for Small Horizontal Axis Wind Turbines", Tech. Rep. [Online]. Available: www.rsisinternational.org/IJRSI.html.

[35] T. Ouyang, A. Kusiak, and Y. He, "Predictive model of yaw error in a wind turbine", *Energy*, 2017, ISSN: 03605442. DOI: 10.1016/j.energy.2017.01.150.

[36] K. Mullen, *Information on Earth's water*, 2019. [Online]. Available: https://www.ngwa.org/what-is-groundwater/About-groundwater/information-on-earths-water.

[37] World Energy Council, "World Energy Resources - Marine Energy 2016", World Energy Council, Tech. Rep., 2016, pp. 1–79. DOI: http://www.worldenergy.org/wp-content/uploads/2013/09/Complete{_}WER{_}2013{_}Survey.pdf. [Online]. Available: https://bit.ly/2F09LZ4.

[38] D. Magagna and A. Uihlein, "Ocean energy development in Europe: Current status and future perspectives", *International Journal of Marine Energy*, 2015, ISSN: 22141669. DOI: 10.1016/j.ijome.2015.05.001.

[39] H. Berg, *Batteries for Electric Vehicles - Materials and Electrochemistry*. Cambridge University Press, 2015, ISBN: 978-1-5231-1344-6.

[40] "Report on Raw Materials for Battery Applications", European Commission, Brussels, Tech. Rep., 2018.

[41] K. Turcheniuk, D. Bondarev, V. Singhal, and G. Yushin, "Ten years left to redesign lithium-ion batteries", *Iraqi Journal of Applied Phsics*, vol. 14, no. 3, pp. 46–47, Jul. 2018. DOI: 10.1038/d41586-018-05752-3. [Online]. Available: http://www.nature.com/articles/d41586-018-05752-3.

[42] C. Banza Lubaba Nkulu, "Sustainability of artisanal mining of cobalt in DR Congo", *Nature Sustainability*, vol. 1, pp. 495–504, 2018. DOI: 10.1038/s41893-018-0139-4D0.

[43] R. A. Huggins, *Energy storage: Fundamentals, materials and applications, second edition*, Second Edition. Springer International Publishing, 2015, pp. 309–322, ISBN: 9783319212395. DOI: 10.1007/978-3-319-21239-5.

[44] G. Albright, J. Edie, and S. Al-Hallaj, "A Comparison of Lead Acid to Lithium-ion in Stationary Storage Applications Published by AllCell Technologies LLC", AllCell Technologies LLC, Tech. Rep., 2012.

[45] M. Lu, F. Beguin, and E. Frackowiak, *Supercapacitors : Materials, Systems and Applications*. John Wiley & Sons, 2013, pp. 69–74, ISBN: 9783527646685.

[46] E. Wikner, "Lithium ion Battery Aging: Battery Lifetime Testing and Physics-based Modeling for Electric Vehicle Applications", PhD thesis, Chalmers University of Technology, 2017.

[47] T. M. Layadi, G. Champenois, M. Mostefai, and D. Abbes, "Lifetime estimation tool of lead-acid batteries for hybrid power sources design", *Simulation Modelling Practice and Theory*, 2015. DOI: 10.1016/j.simpat.2015.03.001.

[48] H. C. Hesse, M. Schimpe, D. Kucevic, and A. Jossen, *Lithium-ion battery storage for the grid - A review of stationary battery storage system design tailored for applications in modern power grids*, 2017. DOI: 10.3390/en10122107.

[49] D. Wang, Y. Bao, and J. Shi, "Online lithium-ion battery internal resistance measurement application in state-of-charge estimation using the extended kalman filter", *Energies*, 2017, ISSN: 19961073. DOI: 10.3390/en10091284.

[50] G. Florides and S. Kalogirou, "Measurements of Ground Temperature at Various Depths", 2004.

[51] D. B. Murray and J. G. Hayes, "Cycle testing of supercapacitors for long-life robust applications", *IEEE Transactions on Power Electronics*, 2015. DOI: 10.1109/TPEL.2014.2373368.

[52] Haisheng Chen, Thang Ngoc Cong, Wei Yang, Chunqing Tan, Yongliang Li, and Yulong Ding, "Progress in electrical energy storage system: A critical

review", *Progress in Natural Science*, vol. 19, no. 3, pp. 291–312, 2009. DOI: https://doi.org/10.1016/j.pnsc.2008.07.014.

[53] R. A. Huggins, *Energy storage: Fundamentals, materials and applications, second edition*, Second Edition. Springer International Publishing, 2015, pp. 95–118, ISBN: 9783319212395. DOI: 10.1007/978-3-319-21239-5.

[54] N. Mohan, T. M. Undeland, and W. P. Robbins, *Power Electronics; Converters, Applications and Design*, 3rd ed. John Wiley & Sons Inc, 2003, pp. 161–200, ISBN: 0-471-42908-2.

[55] K.-H. Chao, M.-C. Tseng, C.-H. Huang, Y.-G. Liu, and L.-C. Huang, "Design and Implementation of a Bidirectional DC-DC Converter for Stand-Alone Photovoltaic Systems", Tech. Rep. 3, 2013.

[56] G. Zhang, Y. Dai, and J. Cui, "Design and Realization of a Bi-directional DC/DC Converter in photovoltaic power system", 2016. DOI: 10.2991/ifeesd-16.2016.197.

A

Appendix 1

A comparison between the theoretical relationship of V_{oc} and I_{sc} with the output power points of the PV system. From figure A.1 it can be seen that a small error exist. For second data point, it can be seen that the error have increased, but decrease for the third point.

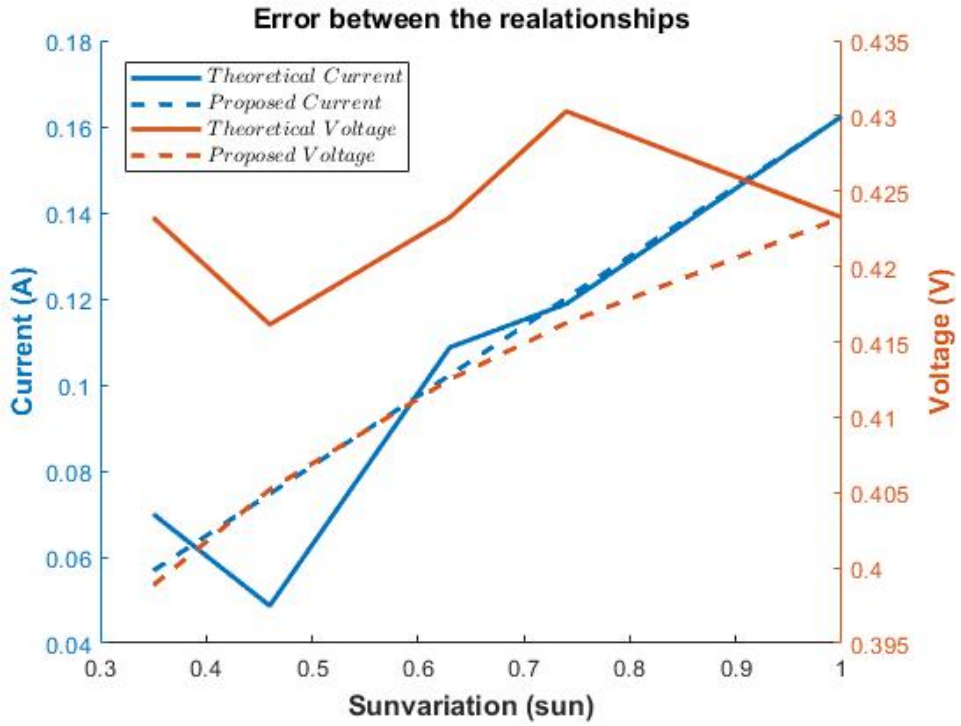

Figure A.1: Display how the error is proposed model is changing depending on the irradiation.

The error from the figure is presented in table A.1 and it is possible to notice that the second data point is more inaccurate compared to other data points.

Table A.1: How the errors are changing with the irradiation for both the voltage and the current.

	350 $[W/m^2]$	460 $[W/m^2]$	630 $[W/m^2]$	740 $[W/m^2]$	1000 $[W/m^2]$
Voltage Error	5.7679%	2.633%	2.5385%	3.2656%	0%
Current Error	18.8142%	-53.3945%	5.9017%	-1.1219%	0%